

Transcriptional changes in specific subsets of *Drosophila* neurons following inhibition of the serotonin transporter

David Krantz (✉ dkrantz@ucla.edu)

UCLA

Shivan Bonanno

<https://orcid.org/0000-0003-1016-9427>

Article

Keywords:

Posted Date: March 17th, 2023

DOI: <https://doi.org/10.21203/rs.3.rs-2626506/v1>

License:   This work is licensed under a Creative Commons Attribution 4.0 International License.

[Read Full License](#)

Additional Declarations: The authors have declared there is **NO** conflict of interest to disclose

1 **Transcriptional changes in specific subsets of *Drosophila* neurons**
2 **following inhibition of the serotonin transporter**

3

4 Bonanno, Shivan L. Ph.D.¹, Krantz, David E. M.D., Ph.D.^{1#}

5

6 ¹Department of Psychiatry and Biobehavioral Sciences, David Geffen School of Medicine,
7 University of California, Los Angeles, CA 90095, USA

8

9 #Correspondence

10

11 David E. Krantz M.D., Ph.D., Professor in Residence

12 3357C Gonda Center for Neuroscience and Genetics

13 David Geffen School of Medicine at UCLA

14 695 Charles Young Drive South, Los Angeles, California 90095-1761

15 Office Phone: 1 310 206 8508

16 Cell Phone: 1 310 869 6526

17 Email: dkrantz@ucla.edu

18

19 Running title: *Drosophila* serotonin

20 **Abstract**

21 The transcriptional effects of SSRIs and other serotonergic drugs remain unclear, in part due to
22 the heterogeneity of postsynaptic cells, which may respond differently to changes in
23 serotonergic signaling. Relatively simple model systems such as *Drosophila* afford more
24 tractable microcircuits in which to investigate these changes in specific cell types. Here, we
25 focus on the mushroom body, an insect brain structure heavily innervated by serotonin and
26 comprised of multiple different but related subtypes of Kenyon cells. We use fluorescence
27 activated cell sorting of Kenyon cells, followed by either or bulk or single cell RNA sequencing to
28 explore the transcriptomic response of these cells to SERT inhibition. We compared the effects
29 of two different *Drosophila* Serotonin Transporter (*dSERT*) mutant alleles as well as feeding the
30 SSRI citalapram to adult flies. We find that the genetic architecture associated with one of the
31 mutants contributed to significant artefactual changes in expression. Comparison of differential
32 expression caused by loss of SERT during development versus aged, adult flies, suggests that
33 changes in serotonergic signaling may have relatively stronger effects during development,
34 consistent with behavioral studies in mice. Overall, our experiments revealed limited
35 transcriptomic changes in Kenyon cells, but suggest that different subtypes may respond
36 differently to SERT loss-of-function. Further work exploring the effects of SERT loss-of-function
37 in other *Drosophila* circuits may be used help to elucidate how SSRIs differentially affect a
38 variety of different neuronal subtypes both during development and in adults.

39

40

41 **Introduction**

42 Though serotonergic neurons comprise only ~1/200,000 neurons in humans, they project to and
43 influence nearly every region of the mammalian brain [1,2], and represent a commonly targeted
44 neurotransmitter system in the treatment of depression [3–6]. The predominant method by
45 which serotonin is cleared from the extracellular space is through reuptake into the presynaptic
46 cell by the plasma membrane serotonin transporter (SERT) [7–10]. SERT is the target of
47 Selective Serotonin Reuptake Inhibitors (SSRIs), which inhibit its activity and thus prolong the
48 availability of extracellular serotonin to bind and activate serotonin receptors (5-HTRs).
49 Widespread prescription of these drugs has motivated many studies of their long-term effects
50 utilizing peripheral samples [11–13] or highly heterogeneous brain tissue [14,15]. However,
51 deeper understanding of serotonergic circuits and their responses to therapeutic interventions
52 remains elusive due in part to the heterogeneity of serotonergic neurons themselves and the
53 cells that they innervate. Such cellular diversity has been highlighted recently in mammals
54 [1,16,17], and a few studies have analyzed gene expression in specific populations of cells
55 postsynaptic to serotonergic neurons [18,19]. Several reports have investigated changes in
56 ribosome-loaded RNA in a particular cell-type after environmental/behavioral perturbations
57 and/or SSRI administration [20,21]. Another recent study has generated multi-omic datasets on
58 fluoxetine vs. sham-treated mice across multiple brain regions, including two datasets utilizing
59 scRNA-seq to analyze specific hippocampal cell types [14]. The complexity of these findings
60 suggests that further, detailed analysis of the response that occurs in different subtypes of
61 neurons will be necessary to fully understand the molecular effects of SERT inhibition.

62

63 Similar to the mammalian CNS, the *Drosophila* brain is innervated by relatively few (~90)
64 broadly projecting serotonergic neurons [22–24]. Due to its relative simplicity, it is much easier
65 to identify structures and circuits in the *Drosophila* brain that are innervated by one or a few,

66 particular serotonergic neurons. This, coupled with the genetic tools available in flies, affords a
67 technically tractable platform for the molecular interrogation of serotonergic circuits and in
68 particular, specific subsets of post-synaptic neurons that receive serotonergic inputs.

69

70 The mushroom bodies (MBs) are structures in the central brain of *Drosophila* and other insects
71 required for learning as well as other behaviors [25]. They are densely innervated by a small
72 number of serotonergic cells [26–31] and are comprised of three major cell subtypes of Kenyon
73 cells (KCs) including α/β , α'/β' , and γ KCs, which can be further subdivided based on
74 morphology, birth order, and gene expression [32,33]. The three major KC subtypes are known
75 to differ in 5-HTR expression profiles [33,34], with 5-HT1A enriched in $KC_{\alpha/\beta}$ and 5-HT1B in KC_{γ}
76 proposed to regulate different behavioral outputs [35–37].

77

78 We have employed bulk RNA-seq as well as single cell RNA-seq following the isolation of KCs,
79 and identify a small number of genes are differentially expressed in the MBs following inhibition
80 of SERT activity. Our results also highlight several technical considerations relevant to the
81 further transcriptional studies of serotonergic circuits.

82

83 **Methods**

84

85 **Fly husbandry and genetic lines**

86 Flies were maintained on a standard cornmeal and molasses-based agar media with a 12:12
87 hour light/dark cycle at room temperature (22–25°C).

88 For experiments involving drug-induced SERT blockade (Fig. 5), female flies were sorted on the
89 day of eclosion and maintained on 1% agar + 5% sucrose + 1% blue food dye, with or without

90 the addition of 3mM citalopram (Sigma, St. Louis, MO, USA, PHR1640), for 4-6 days before
91 dissection.

92 **Fly lines/alleles used**

93 The following fly lines were used in this study are as follows, with stock numbers for lines
94 obtained from the Bloomington *Drosophila* Stock Center (BDSC, Bloomington, Indiana, USA)
95 listed in parentheses: *w¹¹¹⁸* (BDSC:5909), *Mef2-gal4* (BDSC:50742), *UAS-nls.GFP*
96 (BDSC:4776), *dSERT⁴* (gift from H. Schözl), *dSERT¹⁶* (gift from H. Schözl), *dSERT^{TMKO}* (created
97 in this work), DGRP-21 (BDSC:28122), DGRP-129 (BDSC:28141), DGRP-235 (BDSC:28275),
98 DGRP-304 (BDSC:25177), DGRP-320 (BDSC:29654), DGRP-324 (BDSC:25182), DGRP-354
99 (BDSC:55020), DGRP-382 (BDSC:28189), DGRP-383 (BDSC:28190), DGRP-395
100 (BDSC:55022), DGRP-406 (BDSC:29657), DGRP-437 (BDSC:25194), DGRP-461
101 (BDSC:28200), DGRP-819 (BDSC:28242).

102 **FACS and RNA-seq library preparation**

103 Fly lines were constructed as described, bearing *Mef2(P247)-gal4* driving *UAS-nls.GFP* to label
104 Kenyon cell (KC) nuclei. Brains were dissected on the day of eclosion (day 0, Fig. 1-3), or day
105 4-6 (Fig. 4, 5) and the optic lobes removed. Central brains were pooled and dissociated
106 according to previously published methods [38]. The dissociated brain cells were separated by
107 fluorescence-activated cell sorting (FACS) into GFP-positive and GFP-negative isolates using a
108 BD FACS Aria II high-speed cell sorter at the UCLA Jonsson Comprehensive Cancer Center
109 (JCCC) and Center for AIDS Research Flow Cytometry Core Facility [26–31].

110 **Bulk RNA-seq**

111 For each bulk RNA-seq replicate, 18–40 brains were dissected per genotype. Cells were
112 collected directly off FACS (5,900–10,400 GFP⁺ cells per replicate) and lysed immediately in
113 Buffer RLT (Qiagen #79216, Maryland, USA). RNA was purified using a commercial column
114 (RNeasy kit, Qiagen #74034). RNA was stored at -80°C until 5 replicates were collected.
115 Libraries for all samples were prepared simultaneously according to the SMART-seq v2 Ultra
116 Low-input RNA sequencing kit with Nextera XT (Takara Bio, Maryland, USA, v4 #634893),
117 using a protocol adapted from [39–41] and available upon request. Libraries were sequenced
118 with spike-in Phi-X at the UCLA BSRC High Throughput Sequencing Core
119 (<https://stemcell.ucla.edu/high-throughput-sequencing>) on an Illumina NovaSeq SP 2x50bp.
120 After demultiplexing, 24–88 million reads per sample were retained. Quality control was
121 performed using base metrics and nucleotide composition of raw reads. Alignment to
122 the *Drosophila melanogaster* genome (BDGP6) was performed using the STAR spliced read
123 aligner [42] with default parameters. Only uniquely mapped reads were used for subsequent
124 analyses. PCA analysis showed that one pair of samples had modestly increased technical
125 variability, and was removed from subsequent analyses. Differential expression was calculated
126 between mutant and WT samples using DESeq2 [43].

127

128 **scRNA-seq**

129 For each single cell RNA-seq experiment, 7–12 brains were dissected per genotype, and the
130 genotypes pooled for subsequent processing. GFP⁺ cells representing all of the pooled
131 samples were isolated via FACS (6500-10,000 per experiment), collected in Schneider’s media
132 containing BSA, and transported immediately to the UCLA Technology Center for Genomics
133 and Bioinformatics (TCGB) Core Facility (<https://www.uclahealth.org/pathology/tcgb>) for sample
134 processing using the 10x Genomics 3’ GEX v3 platform. For experiments in Fig. 2 (*dSERT*¹⁶,

135 day 0) and Fig. 3 (*dSERT^{TMKO}*, day 0), cells from each experiment were loaded on an individual
136 chip from *10x Genomics*. Similarly, the cells collected experiments in Fig. 4 (*dSERT^{TMKO}*, day 4-
137 6) or Fig. 5 (CIT, day 4-6) were combined into a single sample and loaded onto a single *10x*
138 chip thus reducing variability caused by differences in sample preparation seen in most other
139 RNA-seq methods. For all *10x* chips, the maximum sample volume was loaded, targeting an
140 upper limit of ~10,000 cells. cDNA and libraries were prepared and checked for size distribution
141 by ScreenTape analysis (Agilent Technologies, Carpinteria, CA, USA). Libraries were
142 sequenced on an *Illumina* NovaSeq SP 2x50bp. Raw sequencing reads were processed using
143 Cell Ranger (7.0.0) with default parameters. The reference genome and gene annotations were
144 obtained from FlyBase (6.29). Processed single-cell transcriptomes were demultiplexed based
145 on parental genotypes using demuxlet (version 2, <https://github.com/statgen/popscl>) [44]. In
146 total, genotypes of 14 DGRP strains were used for demultiplexing: DGRP-21, DGRP-129,
147 DGRP-235, DGRP-304, DGRP-320, DGRP-324, DGRP-354, DGRP-382, DGRP-384, DGRP-
148 395, DGRP-406, DGRP-437, DGRP-461, DGRP-819 (<http://dgrp2.gnets.ncsu.edu>) [45]. The
149 genomic coordinates of variants were transformed from the dm3 to the dm6 version of the
150 *Drosophila* reference genome using Crossmap [46]. The following criteria were used to filter
151 variants used for the analysis: (1) only variants residing on chromosome 3 (see Experimental
152 Design); (2) only biallelic single-nucleotide polymorphisms (SNPs) that were called in all
153 analyzed DGRP strains with a maximum non-reference allele count of 2 (i.e. SNPs detected in
154 only one of the strains); (3) the non-DGRP chromosome 3 was analyzed for SNPs that could be
155 shared with DGRP strains, and those variants were removed from the analysis. BAM files from
156 Cell Ranger were used to generate read pileups and to estimate allelic frequencies in our
157 datasets. Alleles detected with high-frequency (i.e. half of the total reads deriving from the 3rd
158 chromosome) are expected to originate from the common non-DGRP chromosome. Only SNPs
159 with minimum coverage of 5 reads and minor-allele frequencies less than 0.2 were kept for the
160 analysis. The processing of the VCF file was performed using VCFtools [47], and SAMtools [48].

161 The final set included 93084 SNPs, which were transformed into heterozygous variants for the
162 demultiplexing of F1 samples (i.e. alleles were modified from 1/1 to 1/0). The same VCF file was
163 used for demultiplexing of all experiments. The genotypes that were not used in a particular
164 experiment/sample were used as negative controls. Raw sequencing reads and the VCF file for
165 demultiplexing will be available at the NCBI repository (upload to GEO in progress).

166 Single-cell data analysis was performed using Seurat (v4.1.1) [49,50]. Single-cell transcriptomes
167 were filtered using the following criteria: (1) transcript count ≥ 1000 ; (2) maximum percentage of
168 mitochondrial transcripts $\leq 20\%$; (3) we also removed cells that were classified by demuxlet as
169 “doublets/ambiguous”, and cells that were assigned to the genotypes that were not used in the
170 given experiment.

171
172 Filtered datasets from all three experiments were analyzed together. First, we integrated all
173 datasets using Seurat V3 workflow with default parameters [49]. The integrated dataset was
174 used for unsupervised clustering using the standard Seurat workflow (principal components:
175 1:10, resolution: 0.3). This analysis revealed 13 clusters, of which 6 expressed markers of
176 Kenyon cells (Supp. Fig. 1A-B). We then removed non- KC clusters and re-ran integration and
177 clustering steps (principal components: 1:10, resolution: 0.1), which yielded 8 transcriptionally
178 distinct populations of KCs. These clusters were annotated based on known marker genes of
179 KC subtypes (Supp. Fig. 1B-C). Three small clusters were present only in one of three
180 experiments and were excluded from further analysis (KC_G3, KC_G4, and KC_AB3).

181
182 Differential gene expression analysis was performed for each KC cluster and each experiment
183 separately using the “pseudobulk” approach [51]. Read counts from single-cell transcriptomes
184 were aggregated at the level of biological replicates (i.e. DGRP strains, see Experimental
185 Design for details). Differential analysis was performed between control and mutant/drug

186 samples using DESeq2 [43]. Differentially expressed genes were identified at adjusted p-value
187 ($p_{\text{adj}} \leq 0.05$ and fold-change ≥ 1.5).

188

189 Data in all figures was processed and plotted using the following R packages: ggplot2 [52],
190 tidyverse [53], ggrepel [54], patchwork [55], nVennR [56], Libra [57], DESeq2 [43], edgeR
191 [58,59], Limma [60], and Seurat [49,50,61].

192

193 **Results**

194

195 To achieve a complete loss of dSERT activity we focused our initial experiments on *dSERT*
196 mutants rather than drug induced blockade. We used previously described flies homozygous for
197 a *P*-element-excision-derived mutant allele (*dSERT*¹⁶) or a genetically-matched control
198 (*dSERT*⁴) with wild-type (WT) dSERT expression [62] (Fig. 1A) and *Mef2(P247)-gal4* [63] driving
199 nuclear-localized GFP to label Kenyon cells. This driver captures most of the KCs across all 3
200 subtypes α/β , α'/β' , and γ [64] but is enriched for α/β and γ relative to α'/β' . We collected female
201 flies on the day of eclosion and dissected brains from *dSERT*⁴ and *dSERT*¹⁶. KCs from each
202 genotype were dissociated in parallel and isolated via FACS using the GFP marker (Fig. 1B). 5
203 replicates per genotype were obtained and bulk RNA-seq libraries (SMART-seq) were prepared
204 for all samples and sequenced together. PCA (data not shown) revealed two samples (one of
205 each genotype) with increased technical variability; these were removed from subsequent
206 analyses.

207

208 Differentially expressed genes (DEGs) between *dSERT*¹⁶ and *dSERT*⁴ samples were identified
209 using DESeq2 [43], and revealed 44 upregulated and 54 downregulated ($p_{\text{adj}} < 0.05$) (Fig. 1C, D
210 and Supp. Table T1). These include DEGs with functions that could represent homeostatic

211 adjustments to perturbations in serotonergic signaling during development, such as transcription
212 factors (*Lim1*, *Achi*), proteins involved in neuronal maturation and development (*Trim9*, *Mis12*)
213 [65,66], a *Drosophila* ortholog of calbindin (*Cbp53E*), ion channels (*Ork1*, *Ppk29*), and other
214 GPCRs (*Dh44-R1*, *Proc-R*, *CCHa2-R*, *Ir76a*) (Fig. 1C, D and Supp. Table T1). When genes
215 were plotted by chromosomal position, however, there was a striking concentration of DEGs on
216 the same arm of the 2nd chromosome (chr2R) as the *dSERT*¹⁶ DNA lesion (Fig 1E). *Drosophila*
217 have only 3 chromosomes that house most of their genome, and some of these observations
218 may represent true findings. However, the buildup on chr2R suggests that at least some of the
219 observations may derive from disruption of genomic DNA rather than changes in serotonergic
220 signaling.

221
222 Though SMART-seq libraries feature increased sensitivity to lowly-expressed transcripts, they
223 necessitate pooling of RNA from all cell-types within the collected population and may result in
224 washout of cell-type specific changes. To investigate the transcriptomics of each KC subtype
225 independently, we followed a recent single cell RNA-seq strategy in which all samples and
226 replicates are pooled and processed together [38,44]. We generated *dSERT*¹⁶ and *dSERT*⁴ fly
227 lines with GFP expressed in KCs as above, but included an additional element unique to each
228 biological replicate: a 3rd chromosome derived from independent WT strains available from the
229 *Drosophila* Genetics Research Panel (DGRP) [45]. Because transcripts derived from DGRP
230 chromosomes bear SNPs, single cells can be bio-informatically traced to genotype-of-origin
231 *post-hoc* (Fig. 2A). This allowed us to pool all replicates of both control and mutant samples for
232 dissociation, FACS, library prep, and sequencing, thereby minimizing long-standing issues of
233 technical variability between individual replicates that contribute to bias in RNA-seq data.
234 Dimensionality reduction (Supp. Fig. S1) resulted in robust clusters for two sub-populations for
235 KC_{α/β} (KC_AB1, KC_AB2), two for KC_γ (KC_G1, KC_G2), and one for KC_{α/β} (KC_ABp1) (Fig.
236 2B). Running pseudobulk differential expression between mutant and control cells collapsed by

237 cell-type revealed 33 significant changes. Some changes were cell-type specific (e.g. *SK* in
238 *KC_G1* and *CG31690* in *KC_AB1*), and many were observed in multiple cell-types (e.g. *prom*,
239 *Cbp53E*, *CG42392*, *Pgant9*) (Fig. 2C, D and Supp. Table T2). For those DEGs that were
240 identified as cell-type specific such as *SK*, we detected robust transcript expression in most of
241 the clusters, lending credence to the hypothesis that the DE observed is in fact specific to a
242 particular cell-type (Supp. Fig. S2). When visualized in pseudo-Manhattan plots (Fig. 2E),
243 however, the bias of DEGs to chr2R was even more pronounced than for SMART-seq (Fig. 1E),
244 highlighting their possible artefactual provenance. The DEGs on chr2R appear to lie in two
245 positional “columns” – one ~7.5 Mb away from *dSERT*, and one that is immediately adjacent to
246 the *dSERT*¹⁶ deletion. One of the DEGs immediately adjacent to the deletion is an eye-specific
247 gene, *prom*, that is not expressed in WT KCs. By extension, we concluded that upregulation of
248 the *prom* transcript in *dSERT*¹⁶ is likely to represent an artefact caused by the deletion of
249 regulatory DNA adjacent to *dSERT* and *prom*.

250

251 To explore the possibility that more precise mutations in *dSERT* might be less disruptive and
252 generate fewer artefactual hits, we generated a new mutant allele using CRISPR [67] to
253 precisely excise ~2.6kb DNA coding for most of the first and second transmembrane domains
254 and simultaneously induce a frameshift in the CDS. We reasoned that even if the resultant
255 mRNA could code for a partial dSERT protein, it would be topologically inverted in the plasma
256 membrane (Fig. 3A). Fly lines bearing the deletion, termed *dSERT*^{TMKO}, were outcrossed six
257 times to *w*¹¹¹⁸. The presence of the deletion was confirmed by PCR-sanger sequencing, and
258 behaviorally in that this line phenocopies the sleep deficit found in *dSERT*¹⁶ (data not shown).
259 We then built fly lines as in the previous experiment, using the new *dSERT*^{TMKO} allele and
260 second chromosomes derived from *w*¹¹¹⁸ as controls, in place of *dSERT*¹⁶ and *dSERT*⁴,
261 respectively. Sample prep, scRNA-seq, and data processing (Fig. 3B) were performed using the
262 same pipeline as for the previous experiment. Again, relatively few (13) DE observations were

263 made between mutant and WT cells (Fig. 3C, Supp. Table T3). However, in this dataset there
264 is no pronounced enrichment of DEGs on chr2R (Fig. 3F). Importantly, some of the DEGs on
265 chr2R in the previous (*dSERT*¹⁶) dataset, including those immediately adjacent to *dSERT*, such
266 as *prom*, are absent from this *dSERT*^{TMKO} dataset (Supp. Fig. S2B). Some genes DE in this
267 experiment were not detected in the previous dataset, such as *LysRS* in multiple cell types and
268 *dpr1* and *mamo* in KC_ABp1 and KC_G2, respectively.

269
270 While it is known that KCs undergo extensive remodeling during pupation [68–72], most of the
271 literature establishing the importance of serotonergic signaling onto them concerns behaviors
272 such as sleep and memory, which are not utilized during pupation. We thus hypothesized that
273 some of the transcriptional changes in response to *dSERT* LOF may not accumulate until the
274 circuit undergoes perturbed activity in the adult fly brain. To assess transcriptional changes that
275 may accumulate after eclosion, we repeated the *dSERT*^{TMKO} scRNA-seq in 4-6 day-old adult
276 flies (Fig. 4A). This experiment yielded a lower cell number per cluster (Supp. Fig. S1F) than
277 those using freshly-eclosed adults, limiting statistical power in calling DE. Nonetheless we
278 observed a small number (15) DEGs between *dSERT*^{TMKO} mutant and WT cells (Fig. 4C,D and
279 Supp. Table T4). Interestingly, some genes (e.g. *LysRS*) were shared with the previous (day 0)
280 dataset, while *Cbp53E*, a gene identified in the *dSERT*¹⁶ day 0 dataset but not found in the
281 *dSERT*^{TMKO} day 0, reappeared in this *dSERT*^{TMKO} day 4-6 dataset.

282
283 The use of constitutive *dSERT* deletion mutants ensures complete and specific SERT LOF, but
284 it is not possible to distinguish between developmental and adult effects. As a first step to study
285 the effects of long-term SERT blockade in circuits that develop normally, we fed adult flies 3mM
286 citalopram (CIT) to pharmacologically inhibit SERT, a concentration that phenocopies the effect
287 of the *dSERT*¹⁶ allele on sleep behavior [62]. After feeding WT flies either CIT or vehicle (VEH)
288 from eclosion for 4-6 days (Fig. 5A), we again isolated GFP-tagged KCs and used single cell

289 seq to assess DE. Similar to the previous two experiments, few genes (6 downregulated and 1
290 upregulated) were identified as DE across any KC subtype between CIT fed and control flies
291 (Fig. 5B-D, Supp. Table T5). As predicted, there was no “pileup” of these observations on
292 chr2R (Fig. 5E).

293

294 To formally assess concordance between the five datasets, we constructed correlation plots
295 displaying pairwise comparisons of the $\log_2(\text{fold-change})$ values for each DE observation. To
296 compare our bulk RNA-seq for *dSERT*¹⁶ vs. *dSERT*⁴ with our first scRNA-seq experiment using
297 the same alleles, we first collapsed all cell-types in the scRNA-seq into one and conducted
298 “pseudobulk” analysis on the entire population of cells. Correlation between these two
299 measures revealed that the bulk RNA-seq picked up many more DEGs (161) than “pseudobulk”
300 from scRNA-seq (26) (Fig. 6A). Many genes, however, exhibited fold-change values of the
301 same sign (up or downreg), even if p_{adj} was only significant in one dataset. Notably, several
302 genes (*Cbp53E*, *otk*, *CG42392*, *Snp*, *RpLP2*, *CG31690*) were concordant between datasets,
303 exclusive of those such as *prom* flagged as artefacts. Next, we compared the *dSERT*¹⁶ and
304 *dSERT*^{TMKO} day 0 scRNA-seq datasets in a similar correlation plot, but retained the cell-type
305 specific DE conducted in the original analysis (Fig. 6B). Again, most DE observations were
306 significant in only one dataset (smaller labels), though *CG42392* was concordant and significant
307 in KC_G1 and KC_G2 in both datasets. Comparison of the *dSERT*^{TMKO} day 0 and day 4-6
308 datasets similarly revealed only concordant changes that were significant in both datasets (Fig.
309 6C), *CG42392* and *LysRS* in KC_G1. Finally, comparison of the *dSERT*^{TMKO} day 4-6 and CIT-
310 fed day 4-6 experiments showed no concordant changes that were significant in both datasets,
311 but many that were significant in one (Fig. 6D).

312

313 **Discussion**

314

315 We have tested whether specific subtypes of post-synaptic cells in a defined serotonergic circuit
316 undergo transcriptional changes in response to the inhibition of dSERT. A large number of
317 previous reports have investigated transcriptomic changes in response to SSRI-like
318 perturbations, but most have used peripheral samples or highly heterogenous brain tissue as
319 input. More recently, specific subtypes of neurons have been targeted using molecular-genetic
320 strategies employed in rodents such as RiboTag [21,73] and untargeted scRNA-seq [14]. We
321 have now employed similar strategies in the fly with an additional purification step – FACS
322 sorting of GFP labeled cells to isolate a genetically-labeled neuronal subtype: the KCs of the
323 mushroom bodies. We have also compared our DE results obtained across two independently-
324 derived, *dSERT* mutant alleles, two different age groups, and against pharmacological SERT
325 inhibition. Our efforts here focusing on KCs have uncovered a small number of possible DEG
326 candidates and defined several experimental pitfalls to consider in the further analysis of
327 serotonergic signaling in the fly. Since the molecular machinery for serotonergic signaling is
328 conserved from flies to humans we speculate that future experiments using similar methods
329 may complement experiments in rodents to determine how different serotonergic circuits
330 respond to inhibition of SERT.

331

332 **Bulk RNA-seq**

333 We initially used a high-sensitivity bulk RNA-seq method (SMART-seq) to profile changes in
334 *dSERT¹⁶* mutant vs. *dSERT⁴* control animals and flies collected on the day they eclosed as
335 adults from pupae (day 0). Since we used a bulk sequencing method, reads from different KC
336 subtypes were analyzed as a group. PCA revealed strong separation of samples by genotype
337 and the elimination of one set of slight outlier samples (data not shown). Standard data
338 processing and calculation of DE revealed 98 DEGs ($p_{\text{adj}} \leq 0.05$). We note that this number is
339 too low for gene ontology (GO) or similar analyses available for *Drosophila* [74,75] (data not
340 shown) and that gene set enrichment analysis (GSEA) is not readily available for *Drosophila*

341 [76]. Importantly, the number of genes we identified is comparable to the number of changes in
342 ribosome-loaded transcripts observed in specific mouse cell types after SSRI treatment,
343 including serotonergic neurons of the raphe nucleus [73], S100a10 corticostriatal neurons [21]
344 and the lower range (48-1243 DEGs) of an additional 27 brain regions recently analyzed in mice
345 [14]. However, we also observed an enrichment of DEGs on chr2R, proximal to the *dSERT*
346 locus, suggesting that their differential expression might be artefactual, and derived from the
347 dysregulation of adjacent or distal DNA affected by the deletion, or perhaps genetic linkage.

348

349 **scRNA-seq**

350 Studies using bulk RNA-seq methods such as SMART-seq are limited by the heterogeneity of
351 the cell-types used for input. In addition, it is known that small differences in sample treatment,
352 even in those processed simultaneously and in parallel, contribute significantly to noise in
353 sequencing data. To address these concerns, we used a newly developed scRNA-seq protocol
354 to “tag” different biological replicates with different DGRP chromosomes, thus allowing them to
355 be processed as a single sample [38]. In the first of these experiments, we again used *dSERT*¹⁶
356 mutant and *dSERT*⁴ control flies at day 0 post-eclosion. We observed an even more
357 pronounced enrichment of DEGs on chr2R proximal to the *dSERT* locus, further suggesting that
358 relatively small changes in genetic architecture can significantly affect the detection of
359 transcriptomic differences.

360

361 To avoid the chromosomal effects of the *dSERT*¹⁶ imprecise excision allele, we generated a
362 new mutant allele using CRISPR/Cas9 (*dSERT*^{TMKO}). In contrast to *dSERT*¹⁶, the *dSERT*^{TMKO}
363 deletion does not include DNA upstream of the start codon that may be more likely to contribute
364 to the regulation of transcription of adjacent genes. We repeated the scRNA-seq experiment at
365 day 0 using *dSERT*^{TMKO} and found that most of the DEGs on ch2R suspected to be artifactual in
366 the *dSERT*¹⁶ dataset were absent in the *dSERT*^{TMKO} dataset, including *prom*, an eye-specific

367 gene 4.3kb upstream of *dSERT*. Together, the data shown in Figs. 2 and 3 indicate that
368 mutations in *dSERT* and other genes used in further analyses should be carefully selected to
369 minimize the disruption of chromosomal architecture.

370

371 Interestingly, one of the few DEGs identified in the *dSERT*^{TMKO} day 0 dataset was *dpr1* in
372 KC_ABp1, a cell-adhesion molecule that may represent an adjustment to dysregulated circuit
373 activity in the presence of aberrant serotonergic signaling. SERT is present in developing
374 serotonergic neurons [77], and SSRIs can cause dysregulation of circuit wiring in mammals [78–
375 80]. Additionally, *Drosophila* serotonergic neurons are remodeled and form new synapses in
376 development [81]. Many cells that express 5-HTRs undergo significant changes in gene
377 expression during this time [38,82] and are further refined by activity [83–85]. It is plausible that
378 other factors involved in circuit formation and stabilization may be targets of homeostatic
379 adjustments in response to altered extracellular serotonin.

380

381 **Adult versus developmental effects of SERT LOF**

382 We hypothesized that loss of dSERT activity during both development and adulthood, rather
383 than development alone, might further alter the DE profile. To test this, we repeated the scRNA-
384 seq protocol using flies that had been aged for 4-6 days rather than freshly-eclosed (day 0). We
385 again observed some changes across multiple cell types (i.e. *LysRS*, *CG42260*), as well as
386 some that were cell-type specific. Among these, the cell surface recognition molecules *beat-IIa*
387 and *side* DE in KC_G2 could, similarly to *dpr1* in KC_AB1 in the experiment with day 0 flies,
388 represent homeostatic changes to maintain proper connectivity. However, the total number of
389 DEGs seen in the aged flies was similar to that seen with newly eclosed flies.

390

391 To further explore the effects of dSERT inhibition in the adult, we fed WT flies the SSRI
392 citalopram (CIT) or vehicle (VEH) for 4-6 days and repeated our scRNA-seq workflow. We

393 uncovered a new set of DEGs, most of which were observed only in the major $KC_{\alpha\beta}$ subtype
394 (KC_{AB1}) and which did not show significant overlap with those detected using mutants. It is
395 possible that off-target effects of CIT dominate these observations, and drug specificity may be
396 tested in future experiments by feeding CIT to *dSERT* mutants. It is also possible that the
397 decrease in SERT activity caused by citalopram was less pronounced than the complete block
398 in activity caused by *dSERT^{TMKO}*, thus reducing the change in serotonergic signaling and the
399 subsequent effects on post-synaptic cells. Alternatively, the very low number of DEGs we detect
400 in adult flies fed citalopram, as well as the relatively small difference in the number of DEGs in
401 day 0 versus day 4-6 *dSERT^{TMKO}* may be consistent with the idea that serotonergic signaling
402 during development exerts more significant changes than inhibition of SERT in the adult.
403 Further genetic methods to knock out *dSERT* during development versus adult flies will be used
404 to address this issue. We note that in mouse models, many effects on behavior seen with both
405 SSRIs and mutants that perturb serotonergic signaling are primarily based on exposure during
406 development [79,86–91].

407

408 **Cell-subtype-specific effects**

409 Some of the DE observed our scRNA-seq experiments appeared to be specific to particular KC
410 types. it is possible that these differences arise from the different expression profiles of 5-HTRs,
411 including the enrichment of 5-HT1A on $KC_{\alpha\beta}$ and 5-HT1B on KC_{γ} . It is also possible that
412 differences in the extent or source of serotonergic innervation of different KC subtypes
413 contributed to these differences. Our data show that although the number of detectable
414 changes in response to *dSERT* LOF is low in this system, even highly similar cell-types (KC
415 subtypes) exhibit different changes in response to the same chronic perturbation. Recent results
416 in mice suggest a similarly heterogenous response in subtypes of hippocampal neurons [14].
417 We suggest that further experiments in the fly will complement studies in mammals to determine

418 the molecular mechanisms by which serotonergic drugs exert their effects on different subsets
419 of neurons.

420

421 **Technical and experimental limitations**

422 Across all of our single cell RNA-seq experiments, both during development and in the adult, the
423 total number of DEGs was lower than those identified in the initial bulk RNA-seq experiment. In
424 contrast to the single cell protocol, SMART-seq captures cells in a chaotropic agent that halts
425 transcriptional dysregulation induced by cell injury and protects RNA from degradation. This
426 difference, and/or differences in library prep methodologies between SMART-seq and 10x
427 3'GEX may have led to better detection of DEGs in our bulk RNA-seq experiment. More
428 generally, it is known that the advantages of scRNA-seq come at the cost of low sequencing
429 depth per cell.

430

431 Several additional factors may contribute to the low number of DE genes we observed in single
432 cell experiments, including relatively low numbers of cells in some clusters (Supp. Fig. S1F).
433 Our power to detect DE was strongest in the clusters with the highest cell number (KC_AB1 and
434 KC_G1) and more cells may be needed to detect subtle changes in gene expression in other
435 subtypes. The stringent nature of our analyses may also have excluded some subtle or variable
436 changes. The percentage of p-values that survived *Benjamini-Hochsberg* multiple comparison
437 correction in each of our scRNA-seq “pseudobulk” analyses was between 2 and 8%. This
438 represents a standard tradeoff in sequencing studies between the unbiased measurement of all
439 genes in the genome at the statistical cost of multiple comparisons. Unfortunately, this also
440 presents a significant barrier in all current studies attempting to identify less consistent or
441 smaller changes. Finally, it is possible that sample prep methodology should be further refined
442 for this type of investigation. For example, in future experiments we will consider alternative

443 methods such as flash freezing tissue [92,93], which may result in a faster and cleaner sample
444 prep with fewer artefactual changes.

445

446 In addition to a relatively small number of DEGs per experiment, comparing our datasets in
447 correlation plots reveals relatively little overlap. This may suggest that genomic background and
448 experimental variability have stronger effects on DE analysis between groups than the effects of
449 dSERT LOF. The least favorable interpretation of this lack of overlap is that most of the DEGs
450 we detected were “noise”, however the stringent statistical analysis suggests otherwise. Based
451 on both the relatively small number of DEGs as well as the relatively limited overlap we observe
452 across experiments, we speculate that the specific post-synaptic cells we chose to study (KCs)
453 may not mount a large transcriptional response to changes in serotonergic signaling. Using the
454 myriad of available drivers to label and isolate different cell types in the fly may reveal different
455 cell types that show more robust transcriptional responses to mutation of *dSERT* or feeding
456 SSRIs than we identified in KCs. In addition, while neuronal excitation and even the signaling
457 cascades modulated by serotonin are known to be intimately linked to transcription [94–96],
458 these pathways are also regulated by many other factors. Serotonergic signaling may only
459 cause weak or microdomain-restricted changes in some pathways, and it is possible that the
460 primary adaptive response to an increase in extracellular serotonin is post-transcriptional.
461 Additional -omic strategies, notably ChIP-seq and ATAC-seq [97,98], have been used with great
462 success from similar starting samples, and provide a complementary approach to RNA-seq in
463 future studies.

464

465 **Candidate genes for further investigation**

466 Despite the low number of observations in this study, those identified may represent a true
467 response to the inhibition of dSERT and changes in extracellular serotonin. If so, they are novel.
468 These include *Cbp53E*, an ortholog of *calbindin* known to affect axon branching in *Drosophila*

469 [99], and *pgant9*, an enzyme involved in sugar-modification of proteins [100,101]. While further
470 validation will be needed, we suggest that concordance across some datasets may justify
471 further investigation of these and other DEGs. In *Drosophila*, testing the functional effects of
472 perturbing candidate genes, rather than additional molecular methods such as RT-PCR or in
473 situ hybridization, may be the most efficient path to testing their validity. The large number of
474 mutants available in the fly as well as the low cost of generating new mutants underscore the
475 power of this approach and its complementary use with RNA-seq studies compared to those
476 conducted other model systems such as rodents.

477

478 **Funding**

479 Funding for this work included R01 MH107390 (DEK), R01 MH114017 (DEK), and a seed grant
480 from the UCLA Depression Grand Challenge (DEK). The funders had no role in study design,
481 data collection and analysis, decision to publish, or preparation of the manuscript.

482

483 **Data Availability**

484 All raw data and Seurat objects generated in this study will deposited on GEO and will be made
485 available upon publication. (Accession number to follow.) No new algorithms were developed in
486 this work

487

488 **Code Availability**

489 Code for data processing and figure creation available upon request.

490

491 **Acknowledgements**

492 The authors wish to thank Yerbol Kurmangaliev for his thoughtful advice and for help
493 demultiplexing and integrating scRNA-seq data. We thank former Krantz Lab graduate student

494 Maureen Sampson, and the Zipursky Lab at UCLA, for help designing experiments. We thank
495 Rebecca Arnold for help dissecting flies in our initial experiments.

496

497 **Contributions**

498 SLB and DEK conceived of and designed all experiments. SLB performed all experiments.

499 SLB performed final computational analysis and generated figures. SLB and DEK wrote the
500 manuscript.

501

502 **Conflicts of interests**

503 There are no competing financial interests in relation to the work described.

504 **References**

- 505 1. Ren J, Isakova A, Friedmann D, Zeng J, Grutzner SM, Pun A, et al. Single-cell
506 transcriptomes and whole-brain projections of serotonin neurons in the mouse dorsal and
507 median raphe nuclei. Marder E, Nelson SB, Gaspar P, editors. eLife. 2019 Oct
508 24;8:e49424.
- 509 2. Charnay Y, Leger L. Brain serotonergic circuitries. Dialogues Clin Neurosci. 2010
510 Dec;12(4):471–87.
- 511 3. Belmaker RH, Agam G. Major Depressive Disorder. N Engl J Med. 2008 Jan 3;358(1):55–
512 68.
- 513 4. Ravindran LN, Stein MB. The pharmacologic treatment of anxiety disorders: a review of
514 progress. J Clin Psychiatry. 2010 Jul;71(7):839–54.
- 515 5. Saravanakumar A, Sadighi A, Ryu R, Akhlaghi F. Physicochemical Properties,
516 Biotransformation, and Transport Pathways of Established and Newly Approved
517 Medications: A Systematic Review of the Top 200 Most Prescribed Drugs vs. the FDA-
518 Approved Drugs Between 2005 and 2016. Clin Pharmacokinet. 2019 Oct 1;58(10):1281–
519 94.
- 520 6. Tanne JH. Antidepressants surpass antihypertensives as most commonly prescribed drugs
521 in US. BMJ. 2009 Aug 19;339:b3380.
- 522 7. Moncrieff J, Cooper RE, Stockmann T, Amendola S, Hengartner MP, Horowitz MA. The
523 serotonin theory of depression: a systematic umbrella review of the evidence. Mol
524 Psychiatry. 2022 Jul 20;1–14.
- 525 8. Kambeitz JP, Howes OD. The serotonin transporter in depression: Meta-analysis of in vivo
526 and post mortem findings and implications for understanding and treating depression. J
527 Affect Disord. 2015 Nov 1;186:358–66.
- 528 9. Hagino Y, Takamatsu Y, Yamamoto H, Iwamura T, Murphy DL, Uhl GR, et al. Effects of
529 MDMA on Extracellular Dopamine and Serotonin Levels in Mice Lacking Dopamine and/or
530 Serotonin Transporters. Curr Neuropharmacol. 2011 Mar;9(1):91–5.
- 531 10. Meyer JH. Imaging the serotonin transporter during major depressive disorder and
532 antidepressant treatment. J Psychiatry Neurosci JPN. 2007 Mar;32(2):86–102.
- 533 11. Beyazyüz M, Albayrak Y, Eğılmez OB, Albayrak N, Beyazyüz E. Relationship between
534 SSRIs and Metabolic Syndrome Abnormalities in Patients with Generalized Anxiety
535 Disorder: A Prospective Study. Psychiatry Investig. 2013 Jun;10(2):148–54.
- 536 12. Halperin D, Reber G. Influence of antidepressants on hemostasis. Dialogues Clin
537 Neurosci. 2007 Mar;9(1):47–59.
- 538 13. Flechtner-Mors M, Jenkinson CP, Alt A, Adler G, Ditschuneit HH. Metabolism in adipose
539 tissue in response to citalopram and trimipramine treatment – An in situ microdialysis
540 study. J Psychiatr Res. 2008 Jun 1;42(7):578–86.

- 541 14. Rayan NA, Kumar V, Aow J, Rastegar N, Lim MGL, O'Toole N, et al. Integrative multi-
542 omics landscape of fluoxetine action across 27 brain regions reveals global increase in
543 energy metabolism and region-specific chromatin remodelling. *Mol Psychiatry*. 2022
544 Nov;27(11):4510–25.
- 545 15. Glover ME, McCoy CR, Shupe EA, Unroe KA, Jackson NL, Clinton SM. Perinatal exposure
546 to the SSRI paroxetine alters the methylome landscape of the developing dentate gyrus.
547 *Eur J Neurosci*. 2019;50(2):1843–70.
- 548 16. Calizo LH, Akanwa A, Ma X, Pan Y zhen, Lemos JC, Craige C, et al. Raphe serotonin
549 neurons are not homogenous: Electrophysiological, morphological and neurochemical
550 evidence. *Neuropharmacology*. 2011 Sep 1;61(3):524–43.
- 551 17. Okaty BW, Commons KG, Dymecki SM. Embracing diversity in the 5-HT neuronal system.
552 *Nat Rev Neurosci*. 2019 Jul;20(7):397–424.
- 553 18. Frazer S, Prados J, Niquille M, Cadilhac C, Markopoulos F, Gomez L, et al. Transcriptomic
554 and anatomic parcellation of 5-HT3AR expressing cortical interneuron subtypes revealed
555 by single-cell RNA sequencing. *Nat Commun*. 2017 Jan 30;8(1):14219.
- 556 19. Winterer J, Lukacsovich D, Que L, Sartori AM, Luo W, Földy C. Single-cell RNA-Seq
557 characterization of anatomically identified OLM interneurons in different transgenic mouse
558 lines. *Eur J Neurosci*. 2019;50(11):3750–71.
- 559 20. Schmidt EF, Warner-Schmidt JL, Otopalik BG, Pickett SB, Greengard P, Heintz N.
560 Identification of the cortical neurons that mediate antidepressant responses. *Cell*. 2012
561 May 25;149(5):1152–63.
- 562 21. Sargin D, Chottekalapanda RU, Perit KE, Yao V, Chu D, Sparks DW, et al. Mapping the
563 physiological and molecular markers of stress and SSRI antidepressant treatment in
564 S100a10 corticostriatal neurons. *Mol Psychiatry*. 2020 May;25(5):1112–29.
- 565 22. Alekseyenko OV, Lee C, Kravitz EA. Targeted Manipulation of Serotonergic
566 Neurotransmission Affects the Escalation of Aggression in Adult Male *Drosophila*
567 *melanogaster*. *PLOS ONE*. 2010 May 24;5(5):e10806.
- 568 23. Monastirioti M. Biogenic amine systems in the fruit fly *Drosophila melanogaster*. *Microsc*
569 *Res Tech*. 1999 Apr 15;45(2):106–21.
- 570 24. Vallés AM, White K. Serotonin-containing neurons in *Drosophila melanogaster*:
571 Development and distribution. *J Comp Neurol*. 1988;268(3):414–28.
- 572 25. Modi MN, Shuai Y, Turner GC. The *Drosophila* Mushroom Body: From Architecture to
573 Algorithm in a Learning Circuit. *Annu Rev Neurosci*. 2020 Jul 8;43(1):465–84.
- 574 26. Scheunemann L, Plaçais PY, Dromard Y, Schwärzel M, Preat T. Dunce
575 Phosphodiesterase Acts as a Checkpoint for *Drosophila* Long-Term Memory in a Pair of
576 Serotonergic Neurons. *Neuron*. 2018 Apr;98(2):350–365.e5.

- 577 27. Coates KE, Calle-Schuler SA, Helmick LM, Knotts VL, Martik BN, Salman F, et al. The
578 Wiring Logic of an Identified Serotonergic Neuron That Spans Sensory Networks. *J*
579 *Neurosci.* 2020 Aug 12;40(33):6309–27.
- 580 28. Coates KE, Majot AT, Zhang X, Michael CT, Spitzer SL, Gaudry Q, et al. Identified
581 Serotonergic Modulatory Neurons Have Heterogeneous Synaptic Connectivity within the
582 Olfactory System of *Drosophila*. *J Neurosci.* 2017 Aug 2;37(31):7318–31.
- 583 29. Dacks AM, Christensen TA, Hildebrand JG. Phylogeny of a serotonin-immunoreactive
584 neuron in the primary olfactory center of the insect brain. *J Comp Neurol.*
585 2006;498(6):727–46.
- 586 30. Suzuki Y, Schenk JE, Tan H, Gaudry Q. A Population of Interneurons Signals Changes in
587 the Basal Concentration of Serotonin and Mediates Gain Control in the *Drosophila*
588 Antennal Lobe. *Curr Biol.* 2020 Mar 23;30(6):1110-1118.e4.
- 589 31. Zhang X, Gaudry Q. Functional integration of a serotonergic neuron in the *Drosophila*
590 antennal lobe [Internet]. *eLife.* eLife Sciences Publications Limited; 2016 [cited 2022 Jul 8].
591 Available from: <https://elifesciences.org/articles/16836/figures>
- 592 32. Tanaka NK, Tanimoto H, Ito K. Neuronal assemblies of the *Drosophila* mushroom body. *J*
593 *Comp Neurol.* 2008;508(5):711–55.
- 594 33. Shih MFM, Davis FP, Henry GL, Dubnau J. Nuclear Transcriptomes of the Seven Neuronal
595 Cell Types That Constitute the *Drosophila* Mushroom Bodies. *G3 Bethesda Md.* 2019 Jan
596 9;9(1):81–94.
- 597 34. Aso Y, Ray RP, Long X, Bushey D, Cichewicz K, Ngo TT, et al. Nitric oxide acts as a
598 cotransmitter in a subset of dopaminergic neurons to diversify memory dynamics.
599 VijayRaghavan K, Ramaswami M, Strauss RH, editors. *eLife.* 2019 Nov 14;8:e49257.
- 600 35. Majeed ZR, Abdeljaber E, Soveland R, Cornwell K, Bankemper A, Koch F, et al.
601 Modulatory Action by the Serotonergic System: Behavior and Neurophysiology in
602 *Drosophila melanogaster*. *Neural Plast.* 2016;2016:7291438.
- 603 36. Ries AS, Hermanns T, Poeck B, Strauss R. Serotonin modulates a depression-like state in
604 *Drosophila* responsive to lithium treatment. *Nat Commun.* 2017 Jun 6;8(1):15738.
- 605 37. Yuan Q, Joiner WJ, Sehgal A. A Sleep-Promoting Role for the *Drosophila* Serotonin
606 Receptor 1A. *Curr Biol.* 2006 Jun 6;16(11):1051–62.
- 607 38. Kurmangaliyev YZ, Yoo J, Valdes-Aleman J, Sanfilippo P, Zipursky SL. Transcriptional
608 Programs of Circuit Assembly in the *Drosophila* Visual System. *Neuron.* 2020
609 Dec;108(6):1045-1057.e6.
- 610 39. Tan L, Zhang KX, Pecot MY, Nagarkar-Jaiswal S, Lee PT, Takemura S ya, et al. Ig
611 Superfamily Ligand and Receptor Pairs Expressed in Synaptic Partners in *Drosophila*.
612 *Cell.* 2015 Dec 17;163(7):1756–69.

- 613 40. Picelli S, Björklund ÅK, Faridani OR, Sagasser S, Winberg G, Sandberg R. Smart-seq2 for
614 sensitive full-length transcriptome profiling in single cells. *Nat Methods*. 2013
615 Nov;10(11):1096–8.
- 616 41. Picelli S, Faridani OR, Björklund ÅK, Winberg G, Sagasser S, Sandberg R. Full-length
617 RNA-seq from single cells using Smart-seq2. *Nat Protoc*. 2014 Jan;9(1):171–81.
- 618 42. Dobin A, Davis CA, Schlesinger F, Drenkow J, Zaleski C, Jha S, et al. STAR: ultrafast
619 universal RNA-seq aligner. *Bioinforma Oxf Engl*. 2013 Jan 1;29(1):15–21.
- 620 43. Love MI, Huber W, Anders S. Moderated estimation of fold change and dispersion for
621 RNA-seq data with DESeq2. *Genome Biol*. 2014 Dec 5;15(12):550.
- 622 44. Kang HM, Subramaniam M, Targ S, Nguyen M, Maliskova L, McCarthy E, et al.
623 Multiplexed droplet single-cell RNA-sequencing using natural genetic variation. *Nat*
624 *Biotechnol*. 2018 Jan;36(1):89–94.
- 625 45. Huang W, Massouras A, Inoue Y, Peiffer J, Ràmia M, Tarone AM, et al. Natural variation in
626 genome architecture among 205 *Drosophila melanogaster* Genetic Reference Panel lines.
627 *Genome Res*. 2014 Jul;24(7):1193–208.
- 628 46. Zhao H, Sun Z, Wang J, Huang H, Kocher JP, Wang L. CrossMap: a versatile tool for
629 coordinate conversion between genome assemblies. *Bioinforma Oxf Engl*. 2014 Apr
630 1;30(7):1006–7.
- 631 47. Danecek P, Auton A, Abecasis G, Albers CA, Banks E, DePristo MA, et al. The variant call
632 format and VCFtools. *Bioinforma Oxf Engl*. 2011 Aug 1;27(15):2156–8.
- 633 48. Li H. A statistical framework for SNP calling, mutation discovery, association mapping and
634 population genetical parameter estimation from sequencing data. *Bioinformatics*. 2011 Nov
635 1;27(21):2987–93.
- 636 49. Stuart T, Butler A, Hoffman P, Hafemeister C, Papalexi E, Mauck WM, et al.
637 Comprehensive Integration of Single-Cell Data. *Cell*. 2019 Jun 13;177(7):1888-1902.e21.
- 638 50. Hao Y, Hao S, Andersen-Nissen E, Mauck WM, Zheng S, Butler A, et al. Integrated
639 analysis of multimodal single-cell data. *Cell*. 2021 Jun 24;184(13):3573-3587.e29.
- 640 51. Squair JW, Gautier M, Kathe C, Anderson MA, James ND, Hutson TH, et al. Confronting
641 false discoveries in single-cell differential expression. *Nat Commun*. 2021 Sep
642 28;12(1):5692.
- 643 52. ggplot2 [Internet]. [cited 2023 Jan 26]. Available from:
644 <https://link.springer.com/book/10.1007/978-3-319-24277-4>
- 645 53. Wickham H, Averick M, Bryan J, Chang W, McGowan LD, François R, et al. Welcome to
646 the Tidyverse. *J Open Source Softw*. 2019 Nov 21;4(43):1686.
- 647 54. Slowikowski K. ggrepel [Internet]. 2022 [cited 2022 Dec 20]. Available from:
648 <https://github.com/slowkow/ggrepel>

- 649 55. Pedersen TL. patchwork [Internet]. 2023 [cited 2023 Jan 26]. Available from:
650 <https://github.com/thomasp85/patchwork>
- 651 56. Pérez-Silva JG, Araujo-Voces M, Quesada V. nVenn: generalized, quasi-proportional Venn
652 and Euler diagrams. *Bioinformatics*. 2018 Jul 1;34(13):2322–4.
- 653 57. neurorestore. README [Internet]. 2023 [cited 2023 Jan 26]. Available from:
654 <https://github.com/neurorestore/Libra>
- 655 58. Robinson MD, McCarthy DJ, Smyth GK. edgeR: a Bioconductor package for differential
656 expression analysis of digital gene expression data. *Bioinformatics*. 2010 Jan 1;26(1):139–
657 40.
- 658 59. McCarthy DJ, Chen Y, Smyth GK. Differential expression analysis of multifactor RNA-Seq
659 experiments with respect to biological variation. *Nucleic Acids Res*. 2012 May
660 1;40(10):4288–97.
- 661 60. Ritchie ME, Phipson B, Wu D, Hu Y, Law CW, Shi W, et al. limma powers differential
662 expression analyses for RNA-sequencing and microarray studies. *Nucleic Acids Res*. 2015
663 Apr 20;43(7):e47.
- 664 61. Butler A, Hoffman P, Smibert P, Papalexi E, Satija R. Integrating single-cell transcriptomic
665 data across different conditions, technologies, and species. *Nat Biotechnol*. 2018
666 May;36(5):411–20.
- 667 62. Knapp EM, Kaiser A, Arnold RC, Sampson MM, Ruppert M, Xu L, et al. Mutation of the
668 *Drosophila melanogaster* serotonin transporter dSERT impacts sleep, courtship, and
669 feeding behaviors. *PLOS Genet*. 2022 Nov 21;18(11):e1010289.
- 670 63. Zars T, Fischer † M., Schulz R, Heisenberg M. Localization of a Short-Term Memory in
671 *Drosophila*. *Science*. 2000 Apr 28;288(5466):672–5.
- 672 64. Aso Y, Grübel K, Busch S, Friedrich AB, Siwanowicz I, Tanimoto H. The Mushroom Body
673 of Adult *Drosophila* Characterized by GAL4 Drivers. *J Neurogenet*. 2009 Jan;23(1–2):156–
674 72.
- 675 65. Yang L, Li R, Kaneko T, Takle K, Morikawa RK, Essex L, et al. Trim9 regulates activity-
676 dependent fine-scale topography in *Drosophila*. *Curr Biol CB*. 2014 May 5;24(9):1024–30.
- 677 66. Zhao G, Oztan A, Ye Y, Schwarz TL. Kinetochores Have a Post-Mitotic Function in
678 Neurodevelopment. *Dev Cell*. 2019 Mar 25;48(6):873–882.e4.
- 679 67. Gratz SJ, Ukken FP, Rubinstein CD, Thiede G, Donohue LK, Cummings AM, et al. Highly
680 Specific and Efficient CRISPR/Cas9-Catalyzed Homology-Directed Repair in *Drosophila*.
681 *Genetics*. 2014 Apr 1;196(4):961–71.
- 682 68. Ganguly A, Qi C, Bajaj J, Lee D. Serotonin receptor 5-HT7 in *Drosophila* mushroom body
683 neurons mediates larval appetitive olfactory learning. *Sci Rep*. 2020 Dec 4;10(1):21267.
- 684 69. Truman JW, Price J, Miyares RL, Lee T. Metamorphosis of memory circuits in *Drosophila*
685 reveal a strategy for evolving a larval brain [Internet]. *bioRxiv*; 2022 [cited 2022 Dec 19]. p.

- 686 2022.06.09.495452. Available from:
687 <https://www.biorxiv.org/content/10.1101/2022.06.09.495452v1>
- 688 70. Kunz T, Kraft KF, Technau GM, Urbach R. Origin of *Drosophila* mushroom body
689 neuroblasts and generation of divergent embryonic lineages. *Development*. 2012 Jul
690 15;139(14):2510–22.
- 691 71. Lee K, Doe CQ. A locomotor neural circuit persists and functions similarly in larvae and
692 adult *Drosophila*. *eLife*. 2021 Jul 14;10:e69767.
- 693 72. Yaniv SP, Schuldiner O. A fly's view of neuronal remodeling. *Wiley Interdiscip Rev Dev*
694 *Biol*. 2016 Sep;5(5):618–35.
- 695 73. Lesiak AJ, Coffey K, Cohen JH, Liang KJ, Chavkin C, Neumaier JF. Sequencing the
696 serotonergic neuron transcriptome reveals a new role for Fkbp5 in stress. *Mol Psychiatry*.
697 2020 May 4;1–12.
- 698 74. Chen EY, Tan CM, Kou Y, Duan Q, Wang Z, Meirelles GV, et al. Enrichr: interactive and
699 collaborative HTML5 gene list enrichment analysis tool. *BMC Bioinformatics*. 2013 Apr
700 15;14:128.
- 701 75. Kuleshov MV, Jones MR, Rouillard AD, Fernandez NF, Duan Q, Wang Z, et al. Enrichr: a
702 comprehensive gene set enrichment analysis web server 2016 update. *Nucleic Acids Res*.
703 2016 Jul 8;44(W1):W90–7.
- 704 76. Cheng J, Hsu LF, Juan YH, Liu HP, Lin WY. Pathway-targeting gene matrix for *Drosophila*
705 gene set enrichment analysis. *PLOS ONE*. 2021 Oct 28;16(10):e0259201.
- 706 77. Ivgy-May N, Tamir H, Gershon M. Synaptic properties of serotonergic growth cones in
707 developing rat brain. *J Neurosci*. 1994 Mar 1;14(3):1011–29.
- 708 78. Van der Knaap N, Wiedermann D, Schubert D, Hoehn M, Homberg JR. Perinatal SSRI
709 exposure affects brain functional activity associated with whisker stimulation in adolescent
710 and adult rats. *Sci Rep*. 2021 Jan 18;11:1680.
- 711 79. Soiza-Reilly M, Meye FJ, Olusakin J, Telley L, Petit E, Chen X, et al. Correction: SSRIs
712 target prefrontal to raphe circuits during development modulating synaptic connectivity and
713 emotional behavior. *Mol Psychiatry*. 2019 May;24(5):773–773.
- 714 80. Simpson KL, Weaver KJ, de Villiers-Sidani E, Lu JYF, Cai Z, Pang Y, et al. Perinatal
715 antidepressant exposure alters cortical network function in rodents. *Proc Natl Acad Sci U S*
716 *A*. 2011 Nov 8;108(45):18465–70.
- 717 81. Roy B, Singh AP, Shetty C, Chaudhary V, North A, Landgraf M, et al. Metamorphosis of an
718 identified serotonergic neuron in the *Drosophila* olfactory system. *Neural Develop*. 2007
719 Oct 24;2(1):20.
- 720 82. Özel MN, Simon F, Jafari S, Holguera I, Chen YC, Benhra N, et al. Neuronal diversity and
721 convergence in a visual system developmental atlas. *Nature*. 2021 Jan;589(7840):88–95.

- 722 83. Sanes JR, Zipursky SL. Synaptic Specificity, Recognition Molecules, and Assembly of
723 Neural Circuits. *Cell*. 2020 Apr 30;181(3):536–56.
- 724 84. Chen Y, Akin O, Nern A, Tsui CYK, Pecot MY, Zipursky SL. Cell-type Specific Labeling of
725 Synapses in vivo through Synaptic Tagging with Recombination (STaR). *Neuron*. 2014 Jan
726 22;81(2):280–93.
- 727 85. Akin O, Bajar BT, Keles MF, Frye MA, Zipursky SL. Cell-type-Specific Patterned Stimulus-
728 Independent Neuronal Activity in the *Drosophila* Visual System during Synapse Formation.
729 *Neuron*. 2019 Mar 6;101(5):894-904.e5.
- 730 86. Zhang Z wei. Serotonin Induces Tonic Firing in Layer V Pyramidal Neurons of Rat
731 Prefrontal Cortex during Postnatal Development. *J Neurosci*. 2003 Apr 15;23(8):3373–84.
- 732 87. Sodhi MSK, Sanders-Bush E. Serotonin and brain development. In: *International Review of*
733 *Neurobiology* [Internet]. Academic Press; 2004 [cited 2023 Feb 13]. p. 111–74. (Disorders
734 of Synaptic Plasticity and Schizophrenia; vol. 59). Available from:
735 <https://www.sciencedirect.com/science/article/pii/S0074774204590062>
- 736 88. Ansorge MS, Morelli E, Gingrich JA. Inhibition of Serotonin But Not Norepinephrine
737 Transport during Development Produces Delayed, Persistent Perturbations of Emotional
738 Behaviors in Mice. *J Neurosci*. 2008 Jan 2;28(1):199–207.
- 739 89. Unroe KA, Maltman JL, Shupe EA, Clinton SM. Disrupted serotonin system development
740 via early life antidepressant exposure impairs maternal care and increases serotonin
741 receptor expression in adult female offspring. *Dev Psychobiol*. 2022;64(6):e22292.
- 742 90. Rebello TJ, Yu Q, Goodfellow NM, Cagliostro MKC, Teissier A, Morelli E, et al. Postnatal
743 Day 2 to 11 Constitutes a 5-HT-Sensitive Period Impacting Adult mPFC Function. *J*
744 *Neurosci*. 2014 Sep 10;34(37):12379–93.
- 745 91. Teissier A, Soiza-Reilly M, Gaspar P. Refining the Role of 5-HT in Postnatal Development
746 of Brain Circuits. *Front Cell Neurosci* [Internet]. 2017 [cited 2022 Jul 5];11. Available from:
747 <https://www.frontiersin.org/articles/10.3389/fncel.2017.00139>
- 748 92. Ma J, Weake VM. Affinity-based Isolation of Tagged Nuclei from *Drosophila* Tissues for
749 Gene Expression Analysis. *J Vis Exp JoVE*. 2014 Mar 25;(85):51418.
- 750 93. Escobedo SE, Stanhope SC, Dong Z, Weake VM. Aging and Light Stress Result in
751 Overlapping and Unique Gene Expression Changes in Photoreceptors. *Genes*. 2022
752 Feb;13(2):264.
- 753 94. Millan MJ, Marin P, Bockaert J, Mannoury la Cour C. Signaling at G-protein-coupled
754 serotonin receptors: recent advances and future research directions. *Trends Pharmacol*
755 *Sci*. 2008 Sep 1;29(9):454–64.
- 756 95. Tyssowski KM, Gray JM. The Neuronal Stimulation-Transcription Coupling Map. *Curr Opin*
757 *Neurobiol*. 2019 Dec;59:87–94.
- 758 96. Pan Y, He X, Li C, Li Y, Li W, Zhang H, et al. Neuronal activity recruits the CRT1/CREB
759 axis to drive transcription-dependent autophagy for maintaining late-phase LTD. *Cell Rep*

- 760 [Internet]. 2021 Jul 20 [cited 2021 Jul 20];36(3). Available from: [https://www.cell.com/cell-](https://www.cell.com/cell-reports/abstract/S2211-1247(21)00796-8)
761 reports/abstract/S2211-1247(21)00796-8
- 762 97. Jain S, Lin Y, Kurmangaliyev YZ, Valdes-Aleman J, LoCascio SA, Mirshahidi P, et al. A
763 global timing mechanism regulates cell-type-specific wiring programmes. *Nature*. 2022
764 Mar;603(7899):112–8.
- 765 98. Jauregui-Lozano J, Bakhle K, Weake VM. In vivo tissue-specific chromatin profiling in
766 *Drosophila melanogaster* using GFP-tagged nuclei. *Genetics*. 2021 Jul 1;218(3):iyab079.
- 767 99. Hagel KR, Beriont J, Tessier CR. *Drosophila* Cbp53E Regulates Axon Growth at the
768 Neuromuscular Junction. *PLOS ONE*. 2015 Jul 13;10(7):e0132636.
- 769 100. Ji S, Samara NL, Revoredo L, Zhang L, Tran DT, Muirhead K, et al. A molecular switch
770 orchestrates enzyme specificity and secretory granule morphology. *Nat Commun*. 2018
771 Aug 29;9(1):3508.
- 772 101. May C, Ji S, Syed ZA, Revoredo L, Daniel EJP, Gerken TA, et al. Differential splicing of
773 the lectin domain of an O-glycosyltransferase modulates both peptide and glycopeptide
774 preferences. *J Biol Chem*. 2020 Aug 28;295(35):12525–36.

775

776 **Figure 1. bulk RNA-seq of KCs, in immediately-eclosed (day 0) flies.** A) The *Drosophila*
777 *dSERT* locus encodes three transcripts (top panel). The *dSERT*¹⁶ mutant bears a 1.1 kb
778 deletion at the 5' end that includes a non-coding exon and upstream regulatory DNA. The
779 *dSERT*⁴ genetic background-matched control contains a 278 bp deletion but does not
780 significantly alter protein expression or behavior compared to WT [62]. B) Sample preparation
781 for bulk sequencing. Flies contained the *Mef2(P247)-gal4* driver and *UAS-nls.GFP* marker for
782 expression in KCs, and were homozygous for either *dSERT*¹⁶ (mutant) or *dSERT*⁴ (control) on
783 the second chromosome. Flies were dissected and pooled by genotype, then dissociated and
784 FACS-sorted in parallel to select for GFP-labeled KCs, followed by isolation of RNA for bulk
785 RNA-seq (SMART-seq). C) Volcano plot showing differential expression between *dSERT*¹⁶ and
786 *dSERT*⁴ groups. DE genes include those encoding the transcription factors *Lim1* and *Achi*, the
787 channels *Ork1* and *Ppk29*, the GPCRs *Dh44-R1*, *Proc-R*, *CCHa2-R*, and *Ir76a*, the calcium
788 binding protein *Cbp53E*, and genes implicated in neuronal development (*Trim9*, *Mis12*). D) The
789 top 50 DE genes are shown as a z-score heatmap. E) DEGs plotted by chromosomal

790 coordinates of genomic locus, with inverse $\log_{10}(p_{\text{adj}})$ on the y-axis. The horizontal dashed line
 791 represents $p_{\text{adj}} \leq 0.05$ cutoff. Most DE genes localize to the same chromosomal arm (chr2R) as
 792 *dSERT* (vertical dashed line).

793

794 **Figure 2. scRNA-seq of KCs from *dSERT*¹⁶ and *dSERT*⁴ flies, in immediately-eclosed (day**

795 **0) flies.** A) Flies used for scRNA-seq contained one of six unique 3rd chromosomes derived
 796 from different DGRP wild-type lines, as well as the markers and *dSERT* alleles used for bulk
 797 seq. Two and four different DGRP lines per group (*dSERT*¹⁶ or *dSERT*⁴, respectively) were
 798 created and served as biological replicates. Brains from all lines were dissected, pooled, and
 799 dissociated together, then FACS-sorted to select KCs used for scRNA-seq. B) t-SNE
 800 dimensional reduction showing distribution of cells in this dataset among transcriptionally-
 801 defined clusters (see methods) representing KC_g cells (KC_G1, KC_G2), KC_{a/b} (KC_AB1,
 802 KC_AB2), and KC_{a/b'} (KC_ABp1). C) Volcano plot from “pseudobulk” analysis (by cluster) of
 803 DEGs between *dSERT*¹⁶ and *dSERT*⁴. Observations are color-coded (as in B) by the KC-type in
 804 which they were identified. D) Venn Diagram showing overlap of DEGs identified in the major
 805 cell clusters. *Cbp53E*, *CG42392*, and *CG33143* were identified as DE in multiple cell types.
 806 E) DEGs plotted by chromosomal locus as in Figure 1E. A skewed localization of DEGs to
 807 chr2R is notable.

808

809 **Figure 3. *dSERT*^{TMKO} scRNA-seq, in immediately-eclosed (day 0) flies.** A) Cartoon depicts

810 the independently-derived *dSERT*^{TMKO} deletion compared to *dSERT*¹⁶. B) Flies used for this
 811 scRNA-seq experiment were homozygous for *dSERT*^{TMKO} or a WT *dSERT* allele derived from
 812 *w*¹¹¹⁸ and expressed with the same transgenes for isolation of KC cells as in Fig 1 and 2. Each
 813 fly was marked by a different DGRP 3rd chromosome variant, and t-SNE plot shows the color-
 814 coded distribution of cells by KC cell-type as in Fig. 2. C) Volcano plot as in Fig. 2C from
 815 “pseudobulk” analysis (by cluster) of DEGs between mutant and control. Observations are color-

816 coded (as in B) by the KC-type in which they were identified. D) Venn Diagram showing overlap
 817 of DEGs identified in the major cell clusters. *CG42392* and *LysRS* were identified as DE in both
 818 KC_G1 and KC_G2. E) DEGs plotted by chromosomal position as in Fig. 2F. In contrast to Fig.
 819 2, observations are not concentrated on chr2R.

820

821 **Figure 4. scRNA-seq for dSERT^{TMKO} vs controls in aged (day 4-6) flies.** A) Flies harboring
 822 the *dSERT^{TMKO}* or WT *dSERT* alleles (in the control line *w¹¹¹⁸*) were aged for 4-6 days then
 823 processed for scRNA-seq as in Figure 3. B) t-SNE plot showing identified cell clusters color-
 824 coded by KC-type. C) Volcano plot as in Figs. 2 and 3C from “pseudobulk” analysis (by cluster)
 825 of DEGs between mutant and control. Cell-type specific DEGs include *beat-Ila* and *side* in
 826 KC_G2, *Myo81F* in KC_G1, *Cbp53E* in KC_AB1 and *LysRS* in KC_G1 and KC_AB1, which was
 827 also DE at day 0. D) Venn Diagram showing overlap of DEGs identified in the major cell
 828 clusters. *LysRS*, *CG42260* and *CG32581* were identified as DE in both KC_AB1 and KC_G1.
 829 E) DEGs plotted by chromosomal position as in Figs. 2 and 3F. Similar to Fig. 3 and in contrast
 830 to Fig. 2, observations are not concentrated on chr2R.

831

832 **Figure 5. scRNA-seq in aged flies treated with an SSRI.** A) Flies with WT *dSERT* alleles
 833 were treated with citalopram (CIT) to block SERT protein activity or vehicle alone (VEH). Each
 834 fly contained one copy of 2nd and 3rd chromosomes derived from a unique DGRP line and
 835 transgenes for marking KCs as in previous figs. B) t-SNE plot indicating the distribution of cells
 836 by cell-type. C) Volcano plot from “pseudobulk” analysis (by cluster) of DEGs between mutant
 837 and control. Cell-type specific DEGs include *Lgr1* and *Ddc* in KC_AB1 and *Hsp26* and *Hsp70Bc*
 838 in KC_G2, none of which were identified in previous experiments. D) Venn Diagram showing
 839 that there is no overlap of DEGs identified in the major cell clusters. E) DEGs plotted by
 840 chromosomal position as in previous figs. Similar to Figs. 3 and 4, observations are not
 841 concentrated on chr2R.

842

843 **Figure 6. Correlation of genes identified as DE between datasets.** A) Correlation plot
 844 showing \log_2 fold-change (L2FC) for DEGs in *dSERT*¹⁶ versus *dSERT*⁴ at day 0, comparing bulk
 845 sequencing (Fig. 1) and the initial scRNA-seq data (Fig. 2) analyzed using “pseudobulk” to
 846 collapse all clusters into one artificial “cell-type” for comparison with the bulk dataset.
 847 Concordant genes significant in both datasets are plotted in a larger font, and colored purple.
 848 Genes significant in only the bulk or scRNA-seq datasets are colored red or blue, respectively.
 849 Diagonal dark grey dashed line represents 1:1 correlation between datasets. The lighter grey
 850 horizontal and vertical lines represent 1.5 fold-change cutoffs for genes of interest.

851 B) Correlation plot between *dSERT*¹⁶ and *dSERT*^{TMKO} day 0 scRNA-seq datasets. Genes are
 852 color-coded by KC type as in previous figures. Genes not significant in either dataset are plotted
 853 with reduced opacity. Genes significant in at least one dataset are plotted with normal opacity.
 854 While there are many genes with L2FC of the same sign in both datasets, most are only
 855 significant in one dataset (smaller labeled points). C) Correlation plot comparing data derived
 856 from newly eclosed (day 0) vs aged flies (day 4-6) using the *dSERT*^{TMKO}. Genes are plotted as
 857 in B. *CG42392* and *LysRS* in KC_G1 were significant in both datasets (larger labels and points),
 858 with DE in the same direction (downregulated). D) Correlation plot between aged *dSERT*^{TMKO}
 859 (d4-6) and aged flies fed citalopram (CIT). One gene (*Hsp26*) was DE in both datasets, although
 860 in a different cell type in each dataset and therefore not highlighted.

861

862 **Supplemental Table T1. DE table for bulk RNA-seq.** Differential expression table (DESeq2)
 863 for bulk RNA-seq shown in Fig. 1, with transcript per million (TPM) for each sample used in
 864 analysis, fold changes, and p-values (raw and adjusted) for each gene. **Filename: bulk_DE.csv**

865

866 **Supplemental Table T2. title: DE table for scRNA-seq, *dSERT*¹⁶ versus *dSERT*⁴, Day 0**
867 **flies.** Differential expression table calculated using the pseudobulk method (collapsed by cell
868 type and genotype) and DESeq2, for scRNA-seq, *dSERT*¹⁶ v *dSERT*⁴, Day 0 shown in Fig. 2.
869 Fold changes, and p-values (raw and adjusted) reported here and below in Supplemental
870 Tables T3-T4. **Filename: scRNA-seq_DEGs_dSERT16_v_dSERT4_Day0.csv**

871
872 **Supplemental Table T3. DE table for scRNA-seq, *dSERT*^{TMKO} versus WT, Day 0 flies.**
873 Differential expression table calculated using the pseudobulk method and DESeq2, for scRNA-
874 seq, *dSERT*-TMKO v WT, Day0 shown in Fig. 3. **Filename: scRNA-seq_DEGs_dSERT-**
875 **TMKO_v_WT_Day0.csv**

876
877 **Supplemental Table T4. DE table for scRNA-seq, *dSERT*^{TMKO} versus WT, Day 4 flies.**
878 Differential expression table calculated using the pseudobulk method and DESeq2, for scRNA-
879 seq, *dSERT*-TMKO v WT, Day4 shown in Fig 4. **Filename: scRNA-seq_DEGs_dSERT-**
880 **TMKO_v_WT_Day4.csv**

881
882 **Supplemental Table T5. DE table for scRNA-seq, citalapram versus vehicle fed Day 4**
883 **flies.** Differential expression table calculated using the pseudobulk method (collapsed by cell
884 type and genotype) and DESeq2, for scRNA-seq, CIT v VEH Day 4 shown in Fig. 5. **Filename:**
885 **scRNA-seq_DEGs_CIT_v_VEH_Day4.csv**

886
887 **Supplemental Figure S1. Clustering and integration for all scRNA-seq experiments**
888 A) Coarse clustering performed on all scRNA-seq datasets, integrated using Seurat. Clusters 4-
889 9 are KCs. B) Expression of marker genes in each cluster, including *prt*, a marker for KCs.
890 Clusters 1,2, and 10-13 are non-neuronal. C) Reclustering of KC's (clusters 4-6 from A),

891 defining transcriptionally-defined subclusters for each KC type. D) Expression of marker genes
892 in each of the clusters from C). E) Final clustering used in DE analysis for all experiments.
893 KC_AB3, KC_G3, and KC_G4 were removed because the number of cells in these clusters was
894 too low to proceed with DE analysis. F) Table showing the number of cells in each cluster, by
895 experiment and genotype.

896

897 **Supplemental Figure S2. Violin plots for selected DEGs from each experiment**

898 A) Violin plots derived from the normalized single-cell dataset examining $dSERT^{16}$ vs $dSERT^4$ at
899 day 0, reflecting the same observations as in Fig. 2C for downregulation and upregulation of
900 genes in different cell types. *Cbp53E* is enriched in KC_AB2, and downregulated in $dSERT^{16}$
901 compared to controls. *SK* is highly expressed in all KC types, but undergoes downregulation in
902 response to $dSERT$ LOF in KC_ABp1 alone. B) Violin plots derived from the normalized single-
903 cell dataset examining $dSERT^{TMKO}$ vs controls at day 0, reflecting the same observations as in
904 Fig. 3C for downregulation and upregulation of genes in different cell types. *LysRS*, identified
905 as downregulated in KC_G1 and KC_G2, is de-enriched in KC_ABp1. Notably, *prom*, is no
906 longer expressed in any cell-type, consistent with the idea that it was an artifact of the $dSERT^{16}$
907 deletion. *Mamo*, identified as DE only in KC_G2, appears to be highly expressed in KC_G1 and
908 KC_ABp1, suggesting that the cell-type specific DE may be a true observation. C) Violin plots
909 derived from the normalized single-cell dataset examining $dSERT^{TMKO}$ vs controls at day 4-6,
910 reflecting the same observations as in Fig. 4C for downregulation and upregulation of genes in
911 different cell types. *LysRS*, identified as downregulated in KC_AB1 and KC_G1, is robustly
912 expressed in the other KC clusters, suggesting that it may be a true cell-type specific change.
913 D) Violin plots derived from the normalized single-cell dataset examining CIT- vs VEH-fed WT
914 flies at day 4-6, reflecting the same observations as in Fig. 5C for downregulation and
915 upregulation of genes in different cell types. *LysRS*, identified as downregulated in KC_AB1

916 and KC_G1, is robustly expressed in the other KC clusters, again suggesting that it may be a
917 true cell-type specific change.

918

919

920

921

922

dSERT locus encodes three transcripts (top panel). The dSERT16 mutant bears a 1.1 kb deletion at the 5' end that includes a non-coding exon and upstream regulatory DNA. The dSERT4 genetic background-matched control contains a 278 bp deletion but does not significantly alter protein expression or behavior compared to WT [62]. B) Sample preparation for bulk sequencing. Flies contained the Mef2(P247)-gal4 driver and UAS-nls.GFP marker for expression in KCs, and were homozygous for either dSERT16 (mutant) or dSERT4 (control) on the second chromosome. Flies were dissected and pooled by genotype, then dissociated and FACS-sorted in parallel to select for GFP-labeled KCs, followed by isolation of RNA for bulk RNA-seq (SMART-seq). C) Volcano plot showing differential expression between dSERT16 and dSERT4 groups. DE genes include those encoding the transcription factors Lim1 and Achi, the channels Ork1 and Ppk29, the GPCRs Dh44-R1, Proc-R, CCHa2-R, and Ir76a, the calcium binding protein Cbp53E, and genes implicated in neuronal development (Trim9, Mis12). D) The top 50 DE genes are shown as a z-score heatmap. E) DEGs plotted by chromosomal *Drosophila* serotonin coordinates of genomic locus, with inverse $\log_{10}(\text{padj})$ on the y-axis. The horizontal dashed line represents $\text{padj} \leq 0.05$ cutoff. Most DE genes localize to the same chromosomal arm (chr2R) as dSERT (vertical dashed line).

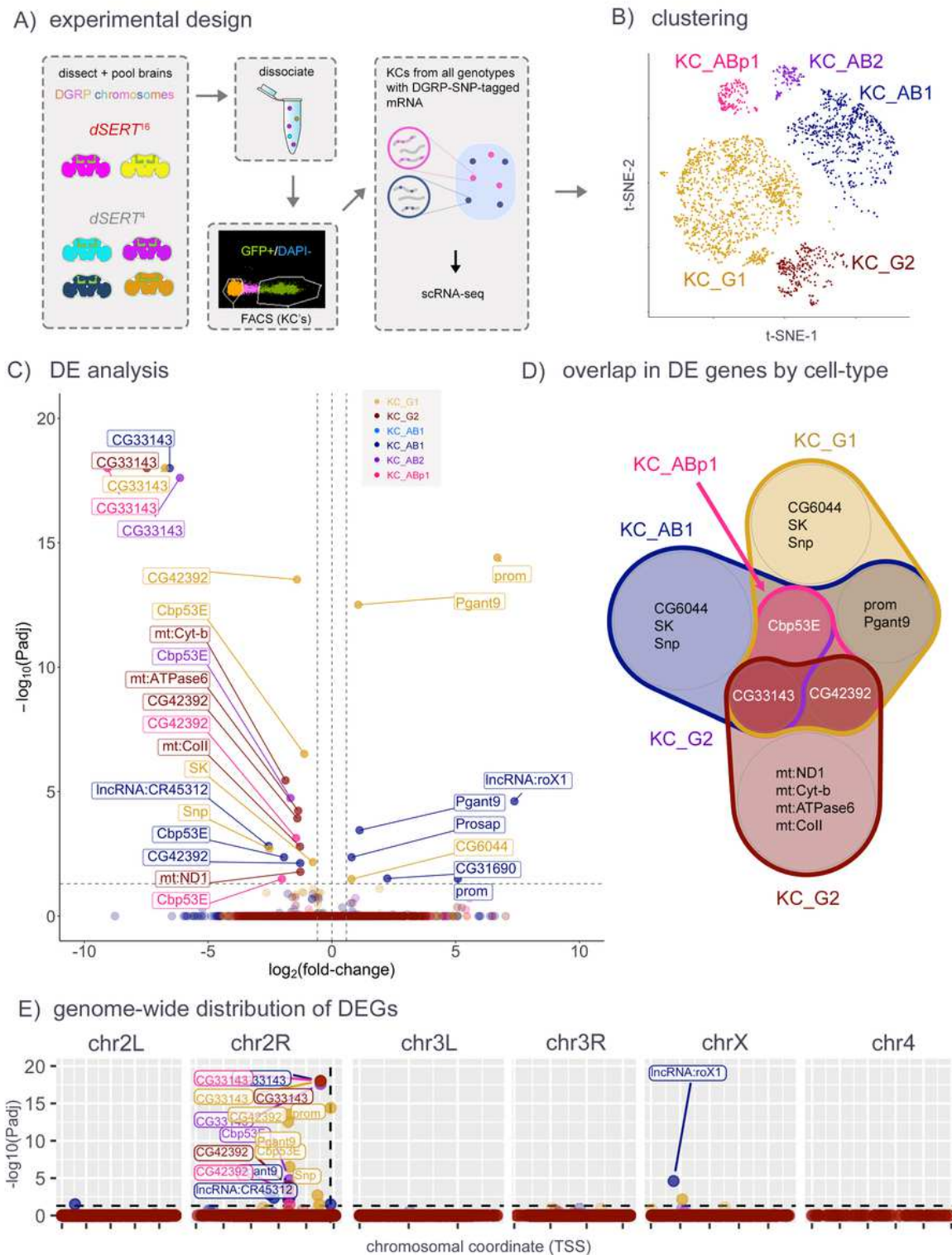


Figure 2

scRNA-seq of KCs from dSERT16 and dSERT4 flies, in immediately-eclosed (day 0) flies.

A) Flies used for scRNA-seq contained one of six unique 3rd chromosomes derived from different DGRP wild-type lines, as well as the markers and dSERT alleles used for bulk seq. Two and four different DGRP lines per group (dSERT16 or dSERT4, respectively) were created and served as biological replicates.

Brains from all lines were dissected, pooled, and dissociated together, then FACS-sorted to select KCs used for scRNA-seq. B) t-SNE dimensional reduction showing distribution of cells in this dataset among transcriptionally- defined clusters (see methods) representing KCg cells (KC_G1, KC_G2), KCa/b (KC_AB1, KC_AB2), and KCa'/b' (KC_ABp1). C) Volcano plot from “pseudobulk” analysis (by cluster) of DEGs between dSERT16 and dSERT4 . Observations are color-coded (as in B) by the KC-type in which they were identified. D) Venn Diagram showing overlap of DEGs identified in the major cell clusters. Cbp53E, CG42392, and CG33143 were identified as DE in multiple cell types. E) DEGs plotted by chromosomal locus as in Figure 1E. A skewed localization of DEGs to chr2R is notable.

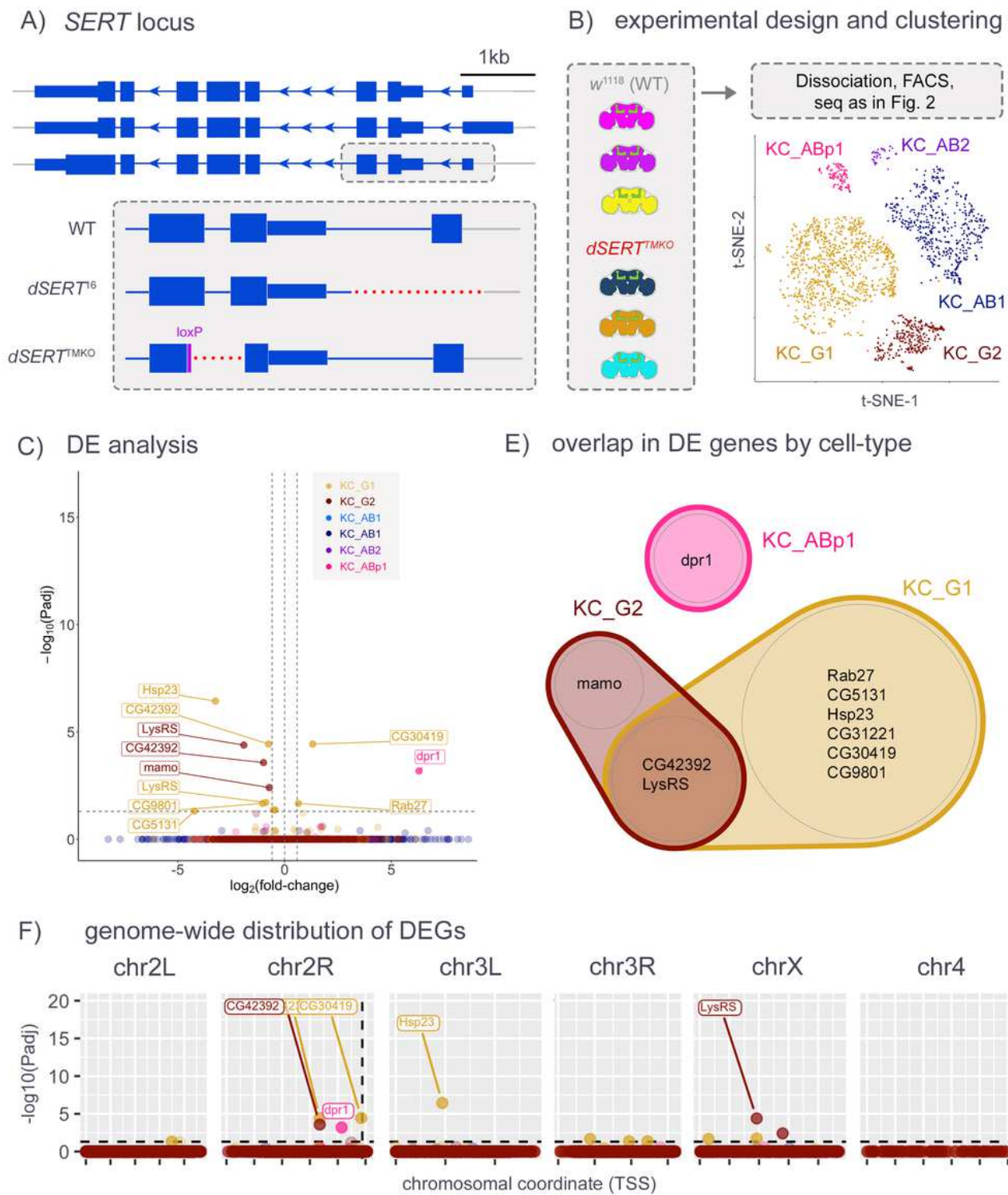


Figure 3

dSERT^{TMKO} scRNA-seq, in immediately-eclosed (day 0) flies.

A) Cartoon depicts the independently-derived dSERT^{TMKO} deletion compared to dSERT¹⁶. B) Flies used for this scRNA-seq experiment were homozygous for dSERT^{TMKO} or a WT dSERT allele derived from w1118 and expressed with the same transgenes for isolation of KC cells as in Fig 1 and 2. Each fly was

marked by a different DGRP 3rd chromosome variant, and t-SNE plot shows the color-coded distribution of cells by KC cell-type as in Fig. 2. C) Volcano plot as in Fig. 2C from “pseudobulk” analysis (by cluster) of DEGs between mutant and control. Observations are color Drosophila serotonin coded (as in B) by the KC-type in which they were identified. D) Venn Diagram showing overlap of DEGs identified in the major cell clusters. CG42392 and LysRS were identified as DE in both KC_G1 and KC_G2. E) DEGs plotted by chromosomal position as in Fig. 2F. In contrast to Fig. 2, observations are not concentrated on chr2R.

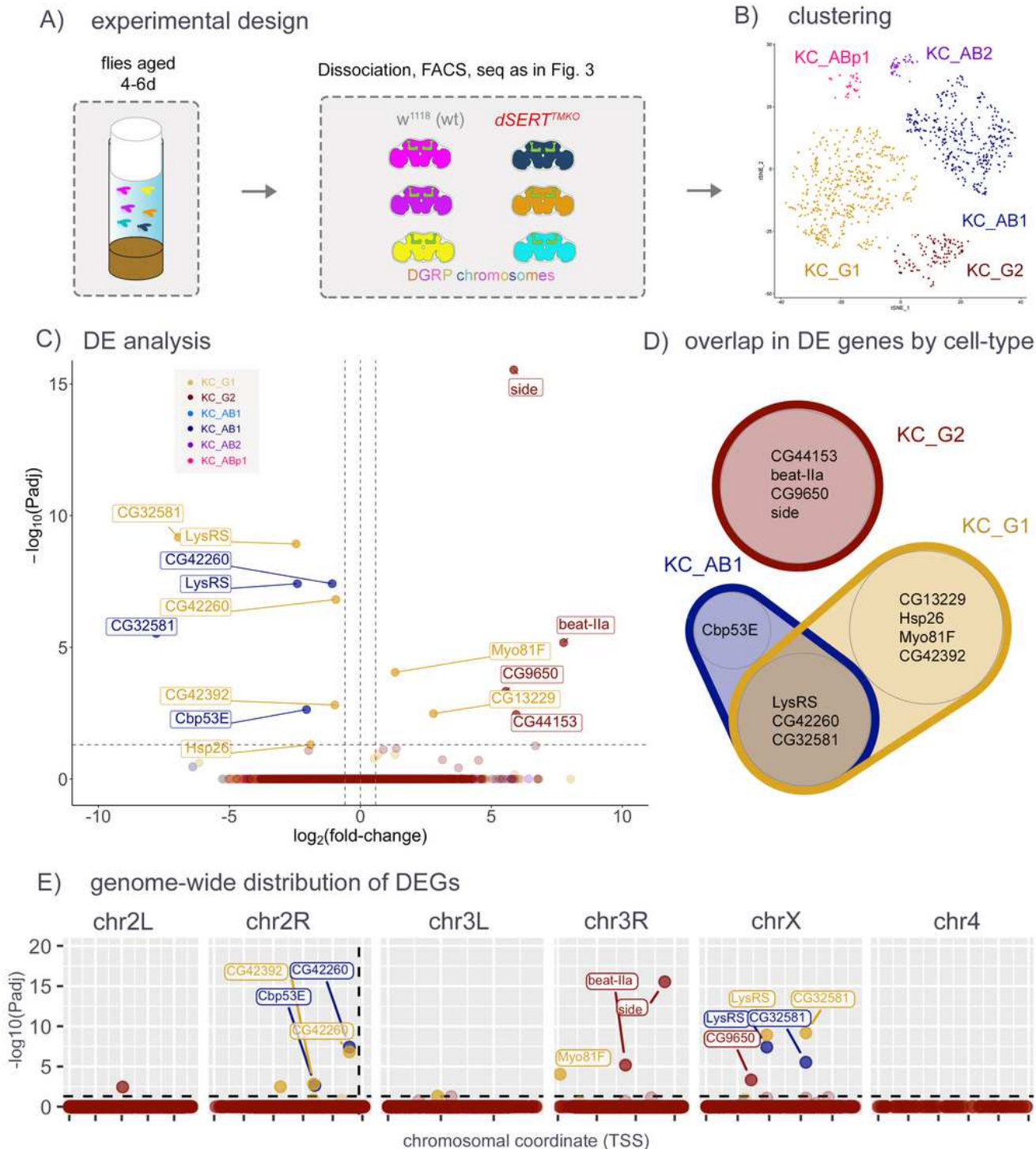


Figure 4

scRNA-seq for dSERTTMKO vs controls in aged (day 4-6) flies.

A) Flies harboring the dSERTTMKO or WT dSERT alleles (in the control line w1118) were aged for 4-6 days then processed for scRNA-seq as in Figure 3. B) t-SNE plot showing identified cell clusters color-coded by KC-type. C) Volcano plot as in Figs. 2 and 3C from “pseudobulk” analysis (by cluster) of DEGs between mutant and control. Cell-type specific DEGs include *beat-IIa* and *side* in KC_G2, *Myo81F* in KC_G1, *Cbp53E* in KC_AB1 and *LysRS* in KC_G1 and KC_AB1, which was also DE at day 0. D) Venn Diagram showing overlap of DEGs identified in the major cell clusters. *LysRS*, CG42260 and CG32581 were identified as DE in both KC_AB1 and KC_G1. E) DEGs plotted by chromosomal position as in Figs. 2 and 3F. Similar to Fig. 3 and in contrast to Fig. 2, observations are not concentrated on chr2R.

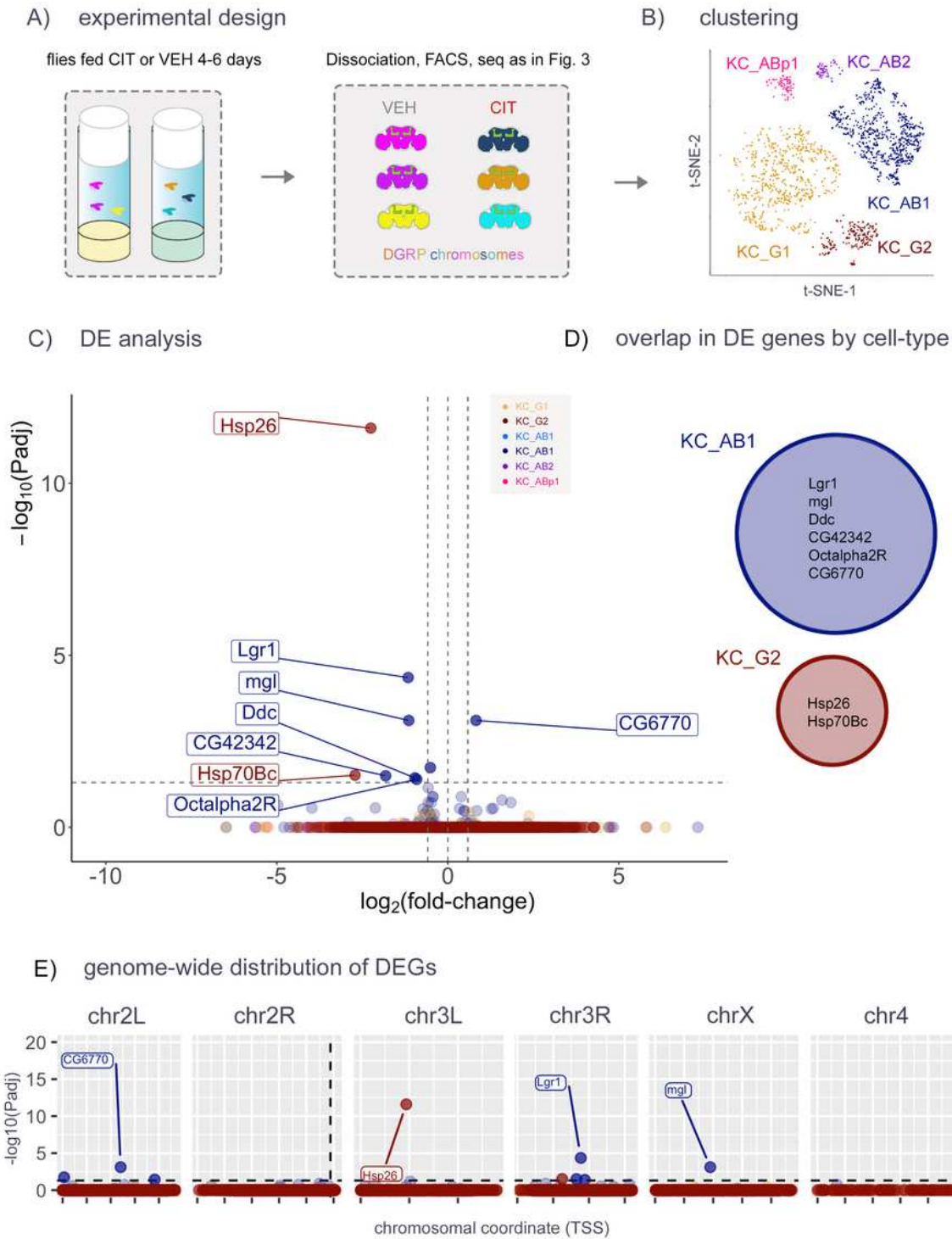


Figure 5

scRNA-seq in aged flies treated with an SSRI.

A) Flies with WT dSERT alleles were treated with citalopram (CIT) to block SERT protein activity or vehicle alone (VEH). Each fly contained one copy of 2nd and 3rd chromosomes derived from a unique DGRP line and transgenes for marking KCs as in previous figs. B) t-SNE plot indicating the distribution of cells by

cell-type. C) Volcano plot from “pseudobulk” analysis (by cluster) of DEGs between mutant and control. Cell-type specific DEGs include *Lgr1* and *Ddc* in *KC_AB1* and *Hsp26* and *Hsp70Bc* in *KC_G2*, none of which were identified in previous experiments. D) Venn Diagram showing that there is no overlap of DEGs identified in the major cell clusters. E) DEGs plotted by chromosomal position as in previous figs. Similar to Figs. 3 and 4, observations are not concentrated on chr2R.

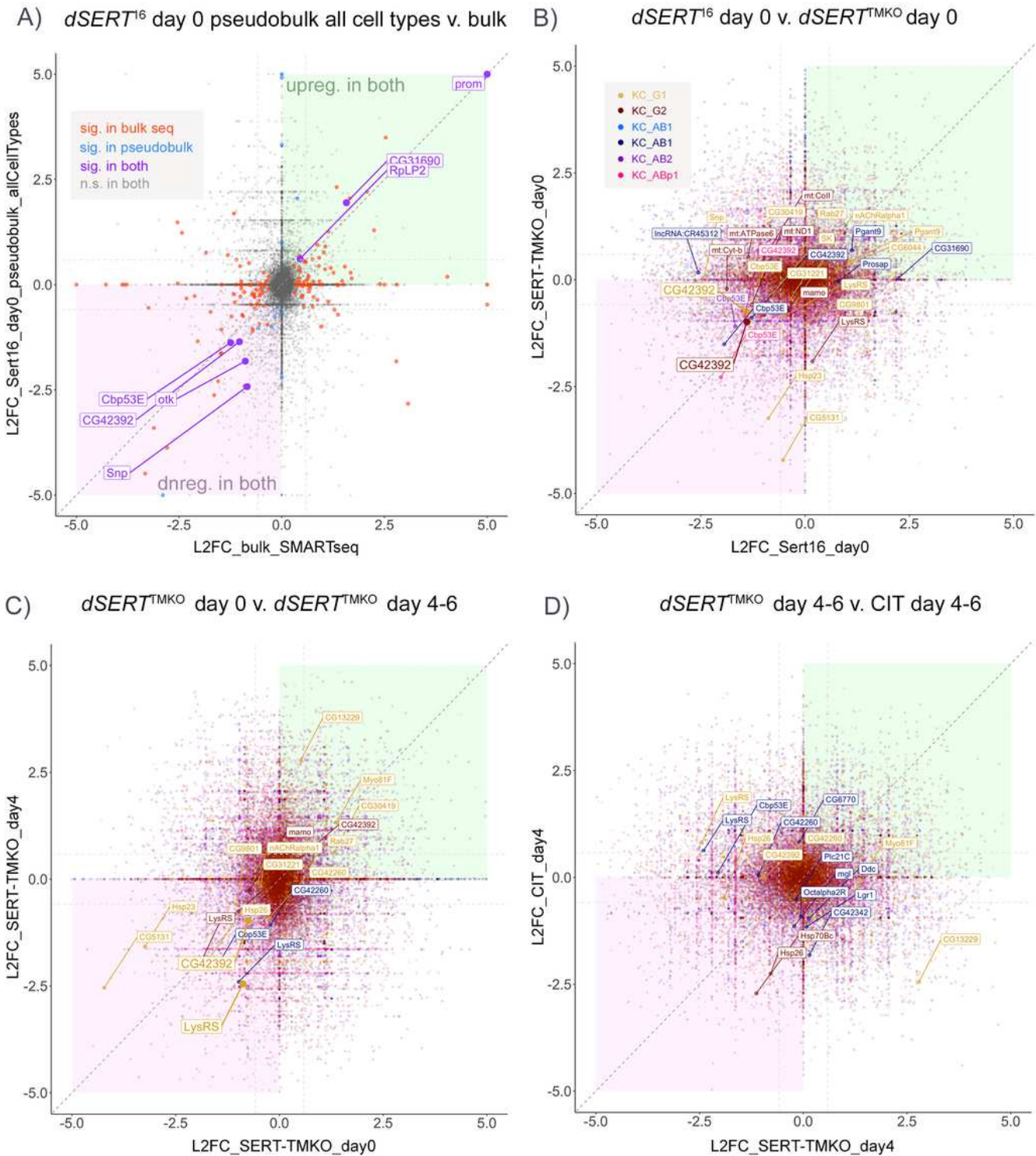


Figure 6

Correlation of genes identified as DE between datasets.

A) Correlation plot showing log₂ fold-change (L2FC) for DEGs in dSERT16 versus dSERT4 at day 0, comparing bulk sequencing (Fig. 1) and the initial scRNA-seq data (Fig. 2) analyzed using “pseudobulk” to collapse all clusters into one artificial “cell-type” for comparison with the bulk dataset. Concordant genes significant in both datasets are plotted in a larger font, and colored purple. Genes significant in only the bulk or scRNA-seq datasets are colored red or blue, respectively. Diagonal dark grey dashed line represents 1:1 correlation between datasets. The lighter grey horizontal and vertical lines represent 1.5 fold-change cutoffs for genes of interest. B) Correlation plot between dSERT16 and dSERTTMKO day 0 scRNA-seq datasets. Genes are color-coded by KC type as in previous figures. Genes not significant in either dataset are plotted with reduced opacity. Genes significant in at least one dataset are plotted with normal opacity. While there are many genes with L2FC of the same sign in both datasets, most are only significant in one dataset (smaller labeled points). C) Correlation plot comparing data derived from newly eclosed (day 0) vs aged flies (day 4-6) using the dSERTTMKO . Genes are plotted as in B. CG42392 and LysRS in KC_G1 were significant in both datasets (larger labels and points), with DE in the same direction (downregulated). D) Correlation plot between aged dSERTTMKO (d4-6) and aged flies fed citalopram (CIT). One gene (Hsp26) was DE in both datasets, although in a different cell type in each dataset and therefore not highlighted.

Supplementary Files

This is a list of supplementary files associated with this preprint. Click to download.

- [FigS1clustering3copy.tif](#)
- [FigS2vlns3copy.tif](#)
- [bulkDE.pdf](#)
- [scRNAseqDEGsdSERT16vdSERT4Day0.pdf](#)
- [scRNAseqDEGsdSERTTMKOvWTDay0.pdf](#)
- [scRNAseqDEGsdSERTTMKOvWTDay4.pdf](#)
- [scRNAseqDEGsCITvVEHDay4.pdf](#)